Accepted Manuscript

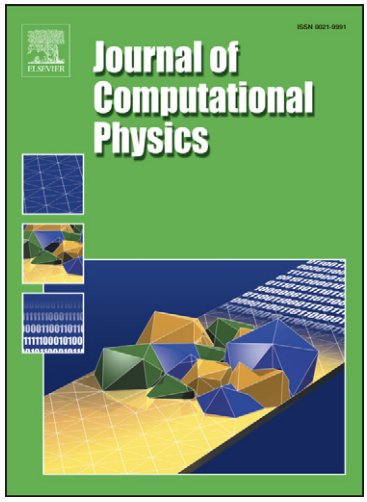

Heterogeneous mixtures of elliptical particles: directly resolving local and global properties and responses

Qianlong Liu, Kenneth L. Reifsnider

PII: S0021-9991(12)00584-0
DOI: http://dx.doi.org/10.1016/j.jcp.2012.09.039
Reference: YJCPH 4247

To appear in: *Journal of Computational Physics*

Received Date: 30 May 2012
Revised Date: 19 September 2012
Accepted Date: 22 September 2012

Please cite this article as: Q. Liu, K.L. Reifsnider, Heterogeneous mixtures of elliptical particles: directly resolving local and global properties and responses, *Journal of Computational Physics* (2012), doi: http://dx.doi.org/10.1016/j.jcp.2012.09.039

This is a PDF file of an unedited manuscript that has been accepted for publication. As a service to our customers we are providing this early version of the manuscript. The manuscript will undergo copyediting, typesetting, and review of the resulting proof before it is published in its final form. Please note that during the production process errors may be discovered which could affect the content, and all legal disclaimers that apply to the journal pertain.

ACCEPTED MANUSCRIPT

Heterogeneous mixtures of elliptical particles: directly resolving local and global properties and responses

Qianlong Liu * and Kenneth L. Reifsnider

DOE Energy Frontier Research Center, Department of Mechanical Engineering, University of South Carolina, Columbia, SC 29208, USA

Abstract

In our earlier papers, Prosperetti's seminal Physalis method for fluid flows was extended to directly resolve electric fields in finite-sized particles and to investigate accurately the mutual fluid-particle, particle-particle, and particle-boundary interactions for circular/spherical particles. For the first time, the method makes the accurate prediction of the local charge distribution, force and torque on finite-sized particles possible. In the present work, the method is extended to heterogeneous mixtures of elliptical particles to further investigate the effects of the orientation and anisotropy. The direct resolution of the effect of fields in heterogeneous mixtures of elliptical particles to determine local and global properties and responses has many applications in engineering, mechanics, physics, chemistry, and biology. The method can be applied to heterogeneous materials, heterogeneous functional materials, microfluidics, and devices such as electric double layer capacitors. In the present paper, the accuracy of the method is extensively investigated even for very challenging problems, for example, for elongated rod-like particles with very high aspect ratios. The accuracy and efficiency of the method suggests that it can be used for many important applications of broad interest.

Key words: Directly resolving particles; elliptical particles; orientation and anisotropy; singularity in elliptic coordinates, local charge distribution; force and torque on particles; discontinuous interface condition; elongated rod-like particle; heterogeneous functional materials; interactions

* Corresponding author.
Email address: liu246@mailbox.sc.edu (Qianlong Liu).

Prosperetti seminally developed the Physalis method [1–3] to directly resolve finite-sized particles in fluid flow [4–7], making it possible to accurately investigate the mutual fluid-particle, particle-particle, and particle-boundary interactions. Recently, we extend the method to electric fields for investigating heterogeneous mixtures of uncharged/charged dielectrics and conductors consisting of up to one million circular or one hundred thousand 3D spherical particles [8,9]. For the first time, the method can be used to predict accurately the local charge distribution, force and torque on particles. The direct resolution is in contrast to the approximate approaches, for example the dielectrophoresis approximation (DEP) in electric fields [10], which assume infinitely small particles without any mutual interactions. In the present paper, we extend the method to elliptical particles to further investigate the effects of orientation and anisotropy that do not appear in circular or spherical particles but are essential to many applications. The present paper provides foundations for further investigations in the direction of non-spherical particles in multiphysics systems.

The motivations for considering elliptical particles in our efforts to model local charge, force, and torque in heterogeneous materials are fundamental, and important to many applications. For field effect transistors, for example, cylindrical nano-wires are known to provide better gate control than any other geometry, and as a result of fabrication methodologies, nano-wire cross sections are generally elliptical in cross section [11]. But available methods for calculating capacitance (which not only determines on-state current but also affects the short-channel characteristics) are restricted to single particle calculations; particle interactions and correct local field calculations (in exact form) have not been reported. Such capabilities are also needed in the field of supercapacitors where electric potential and capacitance computational details are typically restricted to either spherical or (infinitely long) cylindrical geometries [12]. In the field of corrosion, the phenomenon of water uptake is typically represented by the artifice of cylindrical rods of water randomly distributed in the insulating medium [13]. While this is useful for the estimation of the general features of dielectric response in the frequency domain, it does not relate directly to the micro-morphology associated with the fissuring of the substrate or coating [14]. In fact, the authors have discovered that there is a distinct and characteristic relationship between the broadband dielectric spectroscopy response of poorly conductive materials and their micro-defect structure. We have found that there are systematic changes in the dielectric response when progressive changes in that defect structure are induced by time or cycle dependent mechanical loading [15,16]. These micro-defects are micro-cracks, i.e., they are lenticular (or oblate spheroid) regions that become elliptical planar defects when their faces are closed. An example of such cracks

ACCEPTED MANUSCRIPT

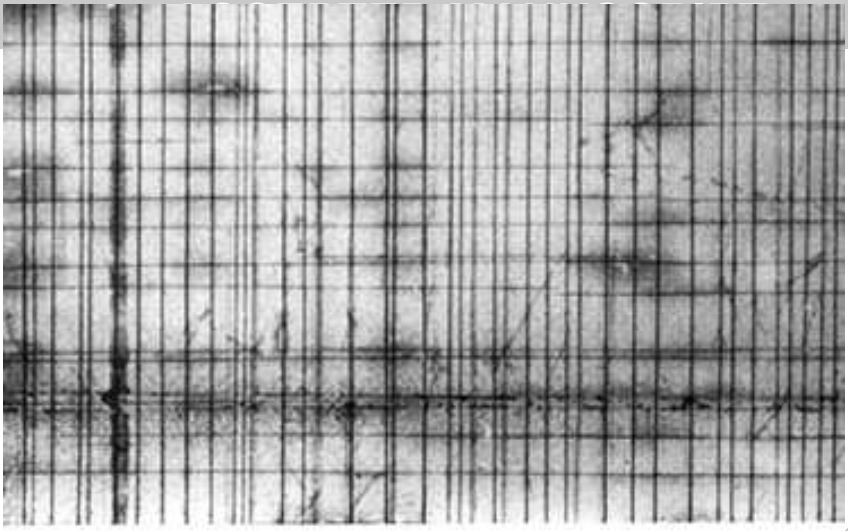

Fig. 1. Microcrack pattern in fiber reinforced polymer composites showing an array of interacting lenticular features (from ref. [17]).

appears in Fig. 1, where lenticular cracks (which appear as dark lines) through the thickness of the plies of that laminate follow the fiber reinforcement directions, and interact to form delamination regions that appear as the shadowy regions at intersections of those cracks [17].

These local interactions are important, since some of the most important dielectric problems in the physical world are associated with the interaction of dielectric regions in a field, i.e., in a static as well as an alternating electric field. If the frequency of the applied field is varied, the "communication" between dielectric regions is established by the inductive field around them. (A simple parallel plate capacitor is an easy analogue.) Reifsnider et al. [18] have shown that the frequency dependence of the response can be interpreted in terms of the local geometry and inductive or conductive connectivity of the included regions. This general concept of frequency dependent material properties, based on dielectric character, is the subject of a remarkably broad spectrum of research that impacts fields as diverse as electrical signal integrity and fibrosis of the human liver [19–21]. More will be said of this frequency dependence in a subsequent publication.

To complete our motivations for the present work, one more class of problems should be mentioned. This class of problems involves heterogeneous functional materials in which one of the constituents may be an active void phase. These materials are called HeteroFoaMs; an example is shown in Fig. 2. HeteroFoaMs are material systems that consist of multiple constituents combined at multiple scales (from nano- to macro-) that actively interact during their functional history in a manner that controls their collective performance as a system at the global level. Examples include composite mixed-conductors, nano- or micro-structured heterogeneous materials, mechanical alloys, nano-structured

ACCEPTED MANUSCRIPT

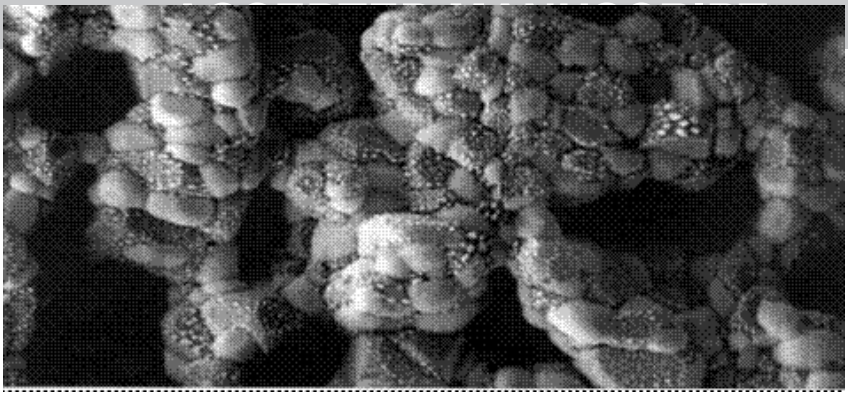

Fig. 2. Example of a heterogeneous functional material, or HeteroFoam, which is an active anode in a solid oxide fuel cell.

interfaces and electrical heterostructures, and many other combinations that typically serve as the heart of engineering devices such as fuel cells, batteries, capacitors, electrolyzers, electrodes, photovoltaics, combustion devices, fuel processing devices, and functional membranes and coatings. The behavior of these materials occurs at multiple scales of time and length and is controlled by multiphysics interactions of the material phases.

HeteroFoam materials are related to heterostructures and heterojunctions which are the heart of many of the semiconductor devices that have changed our society so dramatically [22]. In heterostructures, it is typical, in semiconducting materials for example, to create a material boundary by epitaxially growing one material on the crystalline surface of another, selected in such a way as to create specific alignments of valance and conduction bands in the two materials. However, HeteroFoaMs are heterogeneous functional materials that, unlike familiar heterostructures, involve the co-dependent management, conversion, and transfer of mass, heat and electricity. For a fuel cell, for example, there must be material porosity to transport fuel and air, electrochemical surfaces to oxidize and reduce the reactants, electrically conductive materials (typically both electric and ionic conductors) to create an electric circuit, and material conduits to manage heat flow. This mass transport is fully coupled to the balance of momentum, heat and charge that interactively controls the functionality of the energy device. This distinctive feature of HeteroFoaM materials is responsible for the FoaM part of that acronym, and of special interest to us here, as it defines a genre of functional micro- and nano-structured materials in which the internal geometry, morphology, and connectivity define not only their global properties but their functions. In many cases the functions of HeteroFoaMs involve conduction (e.g., batteries, fuel cells, human tissue), and in general, heterogeneous materials that involve conduction are (as a class) dielectric in some sense [23]. The understanding of the nature, extent, and details of the contribution of material dielectric character to the global functionality of heterogeneous materials, and HeteroFoaMs in particular, is incomplete and poorly codified. The interaction of materials with void

ACCEPTED MANUSCRIPT

ACCEPTED MANUSCRIPT

phases to applied fields is known to be distinctly nonlinear in some cases. Suspensions and foams acted upon by global mechanical stress fields, for example, require that considerations of local moments and rotations be added to classical mechanics descriptions to recover observed behavior in such important functional materials as bone in humans [24,25]. The local torques and forces in heterogeneous functional materials, especially for non-spherical local morphologies, can be calculated, as we will show below, but creating a consistent and coherent global field theory that includes all of the consequences of those local details is still a frontier [26].

In reality, heterogeneous materials in the condensed state, even when man made, rarely (if ever) consist of spheres evenly distributed in a substrate medium with sufficiently dilute density such that the action of applied fields on each particle is independent of the other particles. On the other hand, elliptical shapes bring us one important step closer to a correct representation of many problems of interest. In fact, they introduce critical sensitivity to direction and orientation, aspect ratio, and morphological arrangements that fill space in more realistic ways. Finally, if our analysis is able to capture the details of local field effects when individual elliptical particles are close to each other, we achieve yet another important level of reality in our modeling. Many natural situations involve particles (or distributed regions such as material grains, cracks, etc.) that interact to produce important practical results such as electrical breakdown paths in insulation, micro-to-macro-fracture path development in mechanical fracture, corrosion path development. These, and many other related physical phenomena depend on the interactions of distributed regions for which a precise representation of the local physics that includes non-spherical morphology is essential. The present paper attempts to create a closed form analysis approach to this general class of problems.

In order to directly resolve particles, it is essential to capture all of the local details of the interfaces between the phases, which control many of the system properties and performance. However, the interface conditions make it difficult to construct accurate, efficient, and robust methods. Because of a major advantage of efficient implementation for stationary and moving boundaries with complex geometries, immersed (or embedded) methods have been extensively investigated on underlying fixed Cartesian or structured grids that do not conform to the interface. These methods include the extended finite element methods (XFEM) [27–36], generalized finite element method (GFEM) [37–39], partition of unity finite element method (PUFEM) [40–43], discontinuous enrichment method (DEM) [44–51], virtual node method [52], other finite element methods (FEM) [53–55,32,56], ghost fluid method(GFM) [57–60], immersed interface method(IIM) [61–65], finite volume method(FVM) [66–69], meshfree pseudo-spectral approximation approach [70], matched interface and boundary (MIB) method [71,72], etc. We refer to recent papers [73,74,52,75] for reviews of these numerical methods.

ACCEPTED MANUSCRIPT

The Physalis method is an iterative Immersed Boundary/spectral method [76–79] designed to efficiently and accurately tackle complex geometries. The underlying idea of the Physalis method is to create a cage and to apply a spectral general analytical solution around a discontinuity in a surrounding field to enable the accommodation of physical and geometric discontinuities. The fundamental difference between the Physalis method and above-mentioned other methods is that a spectral general analytical solution is used to satisfied exactly the interface conditions in the former, while penalty methods, Lagrange multipliers, interpolation, or extrapolation are used to enforce the interface conditions in the weak sense or approximately in the latter. It is this difference that results in much more important features regarding derivative quantities, which are typically related to the gradient of the field variable but are much more important for many applications than the field variable. For other methods, the accuracy of the gradient is typically degraded during postprocessing. For example, the gradient decreases to first-order accuracy for a second-order method in a recent paper [52]. In contrast, in the Physalis method, the coefficients in the spectral general analytical solution is even more accurate than the solved field [8,9]. Since the derivative quantities of interest can be expressed simply as algebraic functions of these coefficients, their accuracy does not degrade but rather are more accurate than the solved field. These derivative quantities include local charge distribution, force and torque on the particle, central to many engineering applications. For more details of the advantages and applications of the method, we refer the reader to our recent papers [8,9].

We organize the rest of the paper as follows. In Section 2, the physical problem, corresponding mathematical model, and the numerical method are described. Next, the surface charge distribution, force, and torque are exactly derived in Section 3. The accuracy of the method is validated in Section 4. Finally, the conclusion and future work is discussed in Section 5.

2 Directly resolving elliptical particles using the physalis method

In our recent papers [8,9], heterogeneous mixtures of uncharged/charged dielectrics and conductors are extensively investigated for 2D circular and 3D spherical particles. In the present paper, the algorithm of the Physalis method is extended to elliptical particles. The extension is relatively straightforward, an important advantage with many components of the algorithms shared by the different particle shapes. We focus on the significant difference by introducing non-spherical geometry of the particle, while, for the common components of the algorithm, we refer the reader to the papers [8,9].

ACCEPTED MANUSCRIPT

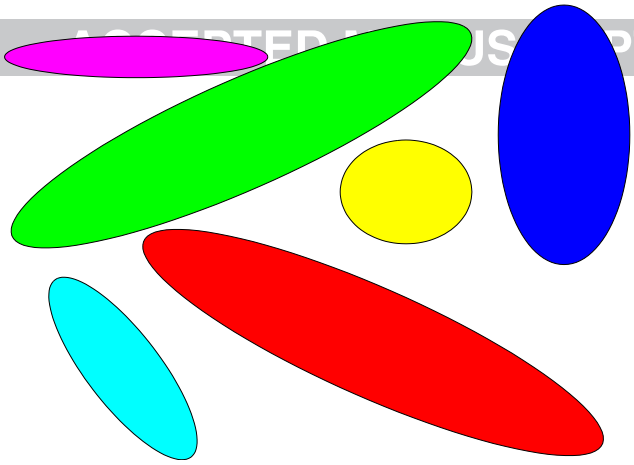

Fig. 3. The situation investigated in the present paper: Heterogeneous mixtures of circular or elliptic dielectric and conductor particles are immersed in the continuous phase in the electric field. These charged/uncharged particles, up to one million and located at arbitrary positions, have arbitrary radii, major and minor axes. Dielectric particles can have arbitrary dielectric constants. Conductor can be simply immersed in the continuous phase or imposed with a voltage by an external source.

2.1 Physical problem, mathematical model, and outline of algorithm

The physical problem investigated is sketched in Fig. 3. Heterogeneous mixtures of non-overlapping circular and elliptic dielectric and conductor particles are immersed in the continuous phase in the electric field. The continuous phase (dispersion medium) has a dielectric constant ϵ^o, where the superscript "o" represents "outside" of the particle, while the charged/uncharged particles, up to one million and denoted with subscript "p", have arbitrary radii, major and minor axes and can be located at arbitrary positions. The dielectric particles have arbitrary dielectric constant ϵ^i, where the superscript "i" represents "inside" the particle. Conductor particles can be simply immersed in the continuous phase or can be introduce with an arbitrary imposed potential V^e, where the superscript "e" means the voltage is provided by an external source. The linear isotropic homogeneity is assumed for both the continuous phase and the particles. The effective dielectric constant includes the contributions from all of the polarization mechanisms.

2.1.1 Governing equation and interface conditions

No free charges exist inside and outside of the particles and thus, the governing equation is the two-dimensional Laplace's equation for the potential $V(x, y)$ in the electric field, where x and y are the original Cartesian coordinates. The potential and coordinates are nondimensionalized with a certain characteristic voltage and length, respectively.

ACCEPTED MANUSCRIPT

At the interface Γ_p between the continuous phase and the p-th particle, discontinuous interface conditions are given by the integral form of the Maxwell equation [80,81]. For each dielectric particle, the interface conditions become

$$V^o = V^i, \ -\epsilon^o \frac{\partial V^o}{\partial n} + \epsilon^i \frac{\partial V^i}{\partial n} = \sigma_f, \tag{1}$$

where n is the surface normal, the specified normalized σ_f is the free charge density at the particle surface and the dielectric constants are normalized by the dielectric constant of a vacuum. For an isolated conductor, initially neutral and then charged with nondimensional electricity Q by the external sources, the interface conditions become:

$$V^o = V^i = const, \ \int \sigma_f dl = Q, \tag{2}$$

where the potential constant is unknown beforehand, the local surface charge distribution is determined by $\sigma_f = -\epsilon^o \frac{\partial V^o}{\partial n}$, and l represents the surface infinitesimal element. For the conductor particle with a specific voltage V^e, the boundary conditions become

$$V^o = V^i = V^e. \tag{3}$$

Note that the method is not limited to these interface conditions but can be applied to the general interface conditions

$$\mathcal{L}\left(\epsilon^o, \epsilon^i, V^o, V^i, \int, \frac{\partial}{\partial n}, \frac{\partial}{\partial l}, \frac{\partial}{\partial x}, \frac{\partial}{\partial y}, \ldots\right) = 0. \tag{4}$$

where $\mathcal{L}$ is a linear operator, involving the field variable, its derivatives, and its integrations, and t is the surface tangential coordinate. The interface conditions with weak discontinuity, strong discontinuity, and strong gradients are just special cases. For more details of the general interface condition, we refer the reader to the recent paper[9].

2.1.2 Surface charge density and force/torque on particles

After the potential is solved under the above interface conditions, the surface charge distribution and force/torque on the particles can be calculated from the first principles. The total surface charges include only free charges for the conductor particle while the bound and free charges for the dielectric particle. The total surface charge density can be written as

ACCEPTED MANUSCRIPT

$$\sigma_t = -\epsilon^o \frac{\partial V^o}{\partial n}, \ \sigma_t = -\frac{\partial V^o}{\partial n} + \frac{\partial V^i}{\partial n}. \tag{5}$$

for the conductor and dielectric particles, respectively. The force and torque exerted on a particle can be written as

$$\vec{F} = \gamma \epsilon^o \int \sigma_t \vec{E}^{o,ext} dl, \ \vec{T} = \gamma \epsilon^o \int \sigma_t \vec{r} \times \vec{E}^{o,ext} dl. \tag{6}$$

For a conductor particle, the coefficient $\gamma = 1/2\epsilon^o$ and the electric field intensity $\vec{E}^{o,ext} = \vec{E}^o = -\nabla V^o$, while for a dielectric particle, $\gamma = 1$ and $\vec{E}^{o,ext} = \vec{E}^{ext}$ includes only external electric field portion of the total field $-\nabla V^o$. It should be noted that, for the dielectric particle, the induced charge on the particle surface cannot exert net force and torque on the particle itself [82–86]. The resultant force and torque from the self contribution should be exactly zero, which cannot be correctly calculated from the surface integration for the induced charge part. For more details, we refer to the textbooks and articles [80–83].

2.1.3 Outline of algorithm

The fundamental difference between the Physalis method and other numerical methods is that a spectral general analytical solution is used to satisfied exactly the discontinuous interface conditions in the former, while penalty methods, Lagrange multipliers, interpolation, or extrapolation are used to enforce the interface conditions in the weak sense or approximately in the latter. In the Physalis method, the computational domain is divided into three regions: a region outside of the particles, a region inside of the particles, and a zone between them used for their coupling. The algorithm to construct the cage in the zone for the elliptical particle is the same as that for circular and spherical particles. For that zone, general analytical solutions are used to"transfer" the interface conditions from the particle surface to the adjacent mesh points, making it possible to avoid the local geometric complexity and insuring that the interface conditions are satisfied exactly. For the region outside of the particles, a standard second-order five-point finite difference scheme for the Laplacian operator is used. The iterations between the analytical and finite-difference solutions yield accurate coefficients for the spectral analytical solutions, making it possible for accurate predictions of local surface charge distribution and force/torque on particles. The algorithm for the elliptical particles is almost identical to that for the circular and spherical particles [8,9], except the general analytical solution in the elliptic coordinates as follows.

ACCEPTED MANUSCRIPT

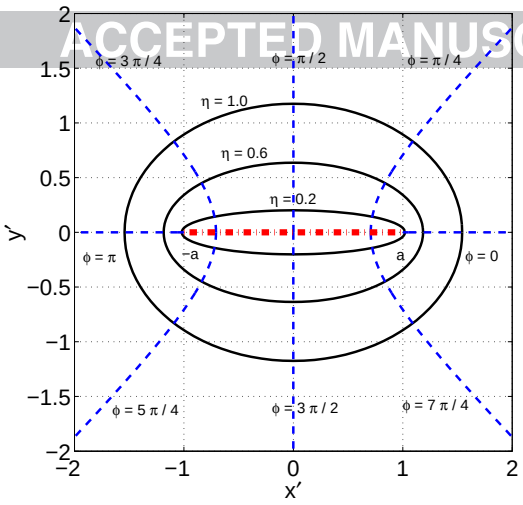

Fig. 4. New Cartesian coordinates (x', y') and elliptic coordinates (η, ϕ): (black) the particle surface $\eta = \text{const}$; (blue) $\phi = \text{const}$; (red) segment between the two foci with singularity, i.e., points $(0, \phi)$ and $(0, 2\pi - \phi)$ collapse.

2.2 Cartesian and elliptic coordinates

Without loss of generality, we consider the p-th particle, whose center is located at (x_p^c, y_p^c) and whose major axis makes an angle Ω_p with the positive x axis in the original Cartesian coordinates (x, y). With the coordinate transformation to the new Cartesian coordinates (x', y')

$$x' = (x - x_p^c)\cos\Omega_p + (y - y_p^c)\sin\Omega_p, \;\; y' = (y - y_p^c)\cos\Omega_p - (x - x_p^c)\sin\Omega_p, \tag{7}$$

its center is located at $(0, 0)$ and its major axis becomes x' axis. As sketched in Fig. 4, the elliptic coordinates (η, ϕ) [87], an orthogonal curvilinear coordinate system, can be defined as

$$x' = a_p \cosh\eta \cos\phi, \;\; y' = a_p \sinh\eta \sin\phi, \tag{8}$$

where $\eta \in [0, \infty)$, $\phi \in [0, 2\pi]$, and the two foci are fixed at $(-a_p, 0)$ and $(a_p, 0)$ in the (x', y') coordinates. The surface of the elliptical particle corresponds to $\eta = \eta_p$ which is specified. Given the coordinates (x', y'), the coordinates (η, ϕ) can be obtained from

$$\sinh^2\eta = \frac{1}{2a_p^2}\left[\sqrt{(a_p^2 - x'^2 - y'^2)^2 + 4a_p^2 y'^2} - (a_p^2 - x'^2 - y'^2)\right], \tag{9}$$

$$\phi = \cos^{-1}(x'/a_p), y' = 0, x' \in [-a_p, a_p]; \;\; \phi = \tan^{-1}\left(\frac{y'\cosh\eta}{x'\sinh\eta}\right). \tag{10}$$

The interface between the p-th elliptical particle and the dispersion phase is specified as, in the (x, y) coordinates,

ACCEPTED MANUSCRIPT

$$\frac{[(x-x_p^c)\cos\Omega_p+(y-y_p^c)\sin\Omega_p]^2}{a_p^2\cosh^2\eta_p}+\frac{[(y-y_p^c)\cos\Omega_p-(x-x_p^c)\sin\Omega_p]^2}{a_p^2\sinh^2\eta_p}=1.$$

For the elliptic coordinate, we denote the square root of the metric coefficients

$$h(\eta,\phi)=\sqrt{g_{11}}=\sqrt{g_{22}}=a_p\sqrt{\cosh^2\eta-\cos^2\phi}, \tag{11}$$

and thus, the infinitesimal distances and the partial differential operator in the normal and tangential directions

$$dn=h(\eta,\phi)d\eta,\ dl=h(\eta,\phi)d\phi,\ \frac{\partial}{\partial n}=\frac{1}{h(\eta,\phi)}\frac{\partial}{\partial\eta}. \tag{12}$$

2.3 Spectral general analytical solutions

In the elliptic coordinates (η,ϕ), the most general solution of the potential field can be written as [87,88]

$$V^g=a_0^g\eta+b_0^g+\sum_{n=1}^{\infty}(a_n^g e^{n\eta}+c_n^g e^{-n\eta})\cos n\phi+(b_n^g e^{n\eta}+d_n^g e^{-n\eta})\sin n\phi, \tag{13}$$

where a_n^g, b_n^g, c_n^g, and d_n^g are coefficients. Note that the terms of $e^{-n\eta}$ result from the induced charge when applied to the external field with the terms of $e^{n\eta}$.

2.3.1 Singularity in the elliptic coordinates

Although the above general solution is valid outside of the particle, it needs to be reduced inside the particle. It should be stressed that, inside the particle, the elliptic coordinate system introduces a singularity in the segment between the two foci, i.e., the coordinates $(0,\phi)$ and $(0,2\pi-\phi)$ represent the same point inside the particle. The singularity, clearly shown in Fig. 4, is essential to reduce the above general solution to avoid nonphysical solutions of Laplace's equation. Unfortunately, to our knowledge, the singularity has not been discussed in the literature, because interests in other physical problems are mainly for solutions outside of the particles.

The fundamental requirement of the existence and continuity of the potential and its first and second derivatives in Laplace's equation (Sec. C), in the neighborhood of the singularity at $\eta=0$ introduces the constraints

ACCEPTED MANUSCRIPT

$$a_0^i = 0,\ c_n^i = a_n^i,\ d_n^i = -b_n^i, \tag{14}$$

yielding the same values for the coordinates $(0, \phi)$ and $(0, 2\pi - \phi)$. The spectral general solutions inside and outside of dielectric/conductor particles are summarized as follows. For details of the derivation, we refer the reader to Sec. B.

2.3.2 General solution in the zone

The general solutions outside of particles are used for the cage points in the zone. From Eq. (A.2) in Sec. A, the weighted surface free charge density in Eq. (1) can be rewritten as the series expansion

$$h(\eta_p, \phi)\sigma_f = \sigma_0 + \sum_{n=1}^{\infty}[\sigma_n^c \cos n\phi + \sigma_n^s \sin n\phi], \tag{15}$$

and the general spectral analytical solution for dielectric particles can be written as

$$\begin{aligned} &V^o + \frac{\sigma_0}{\epsilon^o}\eta - \sum_{n=1}^{\infty} \frac{\cosh n\eta_p e^{n\eta_p} e^{-n\eta}/n}{\epsilon^o \cosh n\eta_p + \epsilon^i \sinh n\eta_p}\sigma_n^c \cos n\phi + \frac{\sinh n\eta_p e^{n\eta_p} e^{-n\eta}/n}{\epsilon^o \sinh n\eta_p + \epsilon^i \cosh n\eta_p}\sigma_n^s \sin n\phi \\ &= b_0 + \sum_{n=1}^{\infty} \frac{(\epsilon^o + \epsilon^i)[e^{n(\eta+\eta_p)} + e^{n(\eta_p-\eta)}] + (\epsilon^o - \epsilon^i)[e^{n(\eta-\eta_p)} + e^{n(3\eta_p-\eta)}]}{\epsilon^o \cosh n\eta_p + \epsilon^i \sinh n\eta_p} 2a_n \cos n\phi \\ &+ \sum_{n=1}^{\infty} \frac{(\epsilon^i + \epsilon^o)[e^{n(\eta+\eta_p)} - e^{n(\eta_p-\eta)}] + (\epsilon^i - \epsilon^o)[e^{n(\eta-\eta_p)} - e^{n(3\eta_p-\eta)}]}{\epsilon^o \sinh n\eta_p + \epsilon^i \cosh n\eta_p} 2b_n \sin n\phi. \end{aligned} \tag{16}$$

The general solution for isolated conductor particles can be written as

$$V^o + \frac{Q}{2\pi\epsilon^o}\eta = b_0 + \sum_{n=1}^{\infty}\left[1 - e^{2n(\eta_p-\eta)}\right] e^{n\eta}\left(a_n \cos n\phi + b_n \sin n\phi\right). \tag{17}$$

The corresponding general solution for conductor with an imposed voltage can be written as

$$V^o - V^e = b_0(\eta - \eta_p) + \sum_{n=1}^{\infty}\left[1 - e^{2n(\eta_p-\eta)}\right] e^{n\eta}\left(a_n \cos n\phi + b_n \sin n\phi\right). \tag{18}$$

Note that the above analytical solutions include all modes. In the numerical implementation, the modes are truncated up to N_c so that there are $2N_c + 1$ total unknown coefficients in the right hand side of the series. The values in the left hand come from the solutions of the finite-difference scheme.

ACCEPTED MANUSCRIPT

2.3.3 General solution inside particle

The general solution for dielectric particles can be written as

$$V^i = -\frac{\sigma_0}{\epsilon^o}\eta_p + b_0 + \sum_{n=1}^{\infty} \frac{(2n\epsilon^o e^{n\eta_p} a_n + \sigma_n^c)\cosh n\eta \cos n\phi}{n(\epsilon^o \cosh n\eta_p + \epsilon^i \sinh n\eta_p)} + \frac{(2n\epsilon^o e^{n\eta_p} b_n + \sigma_n^s)\sinh n\eta \sin n\phi}{n(\epsilon^o \sinh n\eta_p + \epsilon^i \cosh n\eta_p)} \quad (19)$$

The general solution for isolated conductor particles can be written as

$$V^i = b_0 - \frac{Q}{2\pi\epsilon^o}\eta_p, \quad (20)$$

The general solution for a conductor with an imposed voltage can be written as

$$V^i = V^e. \quad (21)$$

These implies that once the convergent solution for the outer is obtained, the coefficients are obtained and the solutions inside the particles are trivially obtained.

3 Surface charge, force, and torque on particles

The convergent results yield accurate coefficients and thus the spectral analytical solutions for V^o and V^i. The accurate results for local surface charge distribution, force, and torque on the conductor/dielectric particles are given. In addition, the theoretical significant effects of orientation and anisotropy on the particles are discussed, by comparing the circular with elliptical particle.

3.1 Circular particles

For details of the local surface charge distribution, force, and torque on the circular/spherical particles, we refer to Sec. E and our recent paper [9]. The results for circular particles using to compare with those for elliptical particles are summarized as follows: (1) Owing to the geometric symmetry of the particles, all of the local quantities are well-behaved on the surface, which means that the field does not have a singular region and its gradients are comparable, making the corresponding numerical simulations relatively easier; (2) The torque on a conductor particle is exactly zero, because the electric field is perpendicular to the particle surface, while the torque on a dielectric particle

ACCEPTED MANUSCRIPT

can become non-zero only when charged; (3) The force results only from the interactions between the adjacent modes n and $n+1$.

3.2 Charge density and electric field intensity at surface

Given the general solution of the potential outside of the isolated conductor particle, Eq. (17), the total surface charge density in Eq. (5) reduces to

$$\frac{h(\eta_p,\phi)}{\epsilon^o}\sigma_t = \frac{Q}{2\pi\epsilon^o} - \sum_{n=1}^{\infty} 2ne^{n\eta_p}(a_n\cos n\phi + b_n\sin n\phi) \tag{22}$$

and the components of the electric field intensity $\vec{E}^o = -\nabla V^o$ at $\eta = \eta_p$

$$\begin{aligned}\frac{4h^2(\eta_p,\phi)}{a_p\sinh\eta_p}E_x =& \frac{Q}{2\pi\epsilon^o}\cos\phi - \sum_{n=1}^{\infty} ne^{n\eta_p}\{[\cos(n-1)\phi+\cos(n+1)\phi]a_n \\ &+[\sin(n-1)\phi+\sin(n+1)\phi]b_n\}, \\ \frac{4h^2(\eta_p,\phi)}{a_p\sinh\eta_p}E_y =& \frac{Q}{2\pi\epsilon^o}\sin\phi - \sum_{n=1}^{\infty} ne^{n\eta_p}\{[\sin(n+1)\phi-\sin(n-1)\phi]a_n \\ &+[\cos(n-1)\phi-\cos(n+1)\phi]b_n\}.\end{aligned}$$

By inserting $Q = -2\pi\epsilon^o b_0$ into the above formulas for isolated conductor, we obtain all results for the case of a conductor with a specific voltage.

Given the general solution of the potential for dielectric particles, Eqs. (16) and (19), the total surface charge density in Eq. (5) reduces to

$$\begin{aligned}h(\eta_p,\phi)\sigma_t =& \frac{\sigma_0}{\epsilon^o} + \sum_{n=1}^{\infty}\frac{4e^{n\eta_p}\sigma_n^c\cos n\phi}{\epsilon^o\cosh n\eta_p+\epsilon^i\sinh n\eta_p} + \frac{4e^{n\eta_p}\sigma_n^s\sin n\phi}{\epsilon^o\sinh n\eta_p+\epsilon^i\cosh n\eta_p} \\ &+\sum_{n=1}^{\infty}2n(\epsilon^o-\epsilon^i)e^{n\eta_p}\left(\frac{\sinh n\eta_p\cos n\phi a_n}{\epsilon^o\cosh n\eta_p+\epsilon^i\sinh n\eta_p} + \frac{\cosh n\eta_p\sin n\phi b_n}{\epsilon^o\sinh n\eta_p+\epsilon^i\cosh n\eta_p}\right)\end{aligned} \tag{23}$$

the x-component of the electric field intensity by the external field at $\eta = \eta_p$ can be written as

$$\begin{aligned}\frac{2h^2(\eta_p,\phi)}{a_p}E_x^{ext} =& -\sum_{n=1}^{\infty}4ne^{n\eta_p}a_n[e^{\eta_p}\cos(n-1)\phi - e^{-\eta_p}\cos(n+1)\phi] \\ &-\sum_{n=1}^{\infty}4ne^{n\eta_p}b_n[e^{\eta_p}\sin(n-1)\phi - e^{-\eta_p}\sin(n+1)\phi],\end{aligned} \tag{24}$$

ACCEPTED MANUSCRIPT

and the y-component of the electric field intensity by the external field can be written as

$$\frac{2h^2(\eta_p,\phi)}{a_p}E_y^{ext} = -\sum_{n=1}^{\infty} 4ne^{n\eta_p}a_n[-e^{\eta_p}\sin(n-1)\phi + e^{-\eta_p}\sin(n+1)\phi]$$
$$-\sum_{n=1}^{\infty} 4ne^{n\eta_p}b_n[e^{\eta_p}\cos(n-1)\phi - e^{-\eta_p}\cos(n+1)\phi]. \quad (25)$$

For brevity, the intermediate steps of the derivations are omitted and we refer to Sec. C for more details.

3.3 Anisotropy effect: particle tip and singularity

The above results of the local surface charge distribution, force, and torque on the elliptic particles show that the surface charge density $\sigma \sim 1/h$ and the electric field intensity $E_{x,y} \sim 1/h^2$, where $h \sim \sinh^2\eta_p + \sin^2\phi \geq 0$. The rest of the terms in the formulas are well-behaved. For the case with a high η_p value, for example $\eta_p = 1.0$ in Fig. 4, all of these terms are well-behaved on the surface. This is similar to a circular particle case, because the anisotropy is weak.

In contrast, for the case with a low η_p value, the anisotropy effect becomes very strong. At the particle tip $\phi = 0, \pi$, the Taylor expansion yields the surface charge density and electric field of the respective order $1/\eta_p$ and $1/\eta_p^2$ approaching to ∞ as $\eta_p \to 0$, while away from the singular region, all terms are well-behaved with $h \sim 1$. The discrepancy up to two orders of magnitude of the field results from the strong anisotropy, showing that both the surface charge density and electric electric field (i.e. the gradient of the potential field) are very strong at the particle tip while they are much weaker in the rest region. This feature implies one of the difficulties to numerically calculate the elliptical particles, which is in contrast to circular/spherical particles which do not have this kind of singularity. Therefore, these kinds of problems are very challenging for any numerical method and there are very few results reported in literature. In particular, for very high aspect ratio (AR), the ratio of the major and minor semi-axes $a_p\cosh\eta_p/a_p\sinh\eta_p$, it is extremely difficult to directly resolve the particle, especially to efficiently resolve the tip region for the accurate prediction of the local charge, force, and torque, which, nevertheless, dominates the behavior of the particle. In the present paper, we show the case with AR as high as 100.

We also note that the modes for the surface charge density and electric field share the same forms for the circular and elliptical particles. For example, E_x is contributed from $\cos(n\pm1)\phi a_n$ and $\sin(n\pm1)\phi b_n$.

ACCEPTED MANUSCRIPT

Eq. (6) gives the force and torque in term of the surface integrations at $\eta = \eta_p$

$$\vec{F} = \gamma\epsilon^o \int_0^{2\pi} d\phi \frac{1}{h^2(\eta_p,\phi)} (h\sigma_t) \left(h^2 E_x \hat{x} + h^2 E_y \hat{y}\right), \ \vec{T} = \gamma\epsilon^o \int_0^{2\pi} d\phi \frac{1}{h^2(\eta_p,\phi)} (h\sigma_t) (h^2 L_z) \quad (26)$$

where $\vec{L} = \hat{r} \times (-\nabla V^o)$. It can be shown that, for a conductor,

$$\frac{4h^2(\eta_p,\phi)}{a_p^2} L_z = \frac{Q}{\pi\epsilon^o} \sin 2\phi$$
$$- \sum_{n=1}^{\infty} 2ne^{n\eta_p} [a_n(\sin(n+2)\phi - \sin(n-2)\phi) + b_n(\cos(n-2)\phi - \cos(n-2)\phi)] \quad (27)$$

and that, for a dielectric from the external field,

$$\frac{4h^2(\eta_p,\phi)}{a_p^2} L_z^{ext} = \sum_{n=1}^{\infty} 4ne^{n\eta_p} a_n [-\sin(n+2)\phi + \sin(n-2)\phi + (e^{2\eta_p} - e^{-2\eta_p})\sin\phi]$$
$$- \sum_{n=1}^{\infty} 4ne^{n\eta_p} b_n [-\cos(n+2)\phi + \cos(n-2)\phi + (e^{2\eta_p} - e^{-2\eta_p})\cos\phi]. \quad (28)$$

We refer to Sec. C for more details of the derivation. By comparing with the formula for the circular particle in Sec. E, the elliptical and circular particles share the modes of $\sin n\phi a_n$ and $\cos n\phi b_n$. However, different from the circular particle, there are extra mode contributions to the torque such as $\sin(n\pm2)\phi a_n$ and $\cos(n\pm2)\phi b_n$, resulting from the fact that the surface normal is not parallel to $\vec{r}$ also shown in Sec. C.

One of the major differences between the circular/spherical and elliptical particles is that, for the latter, the electric field intensity, the surface charge density, and L_z are in the form of weighted Fourier series. Unfortunately, this difference makes the straightforward surface integration for the force and torque impossible by using the formula for the integration of the product of two functions in Sec. A as did for circular/spherical particles. One option is to numerically integrate the weighted product of two Fourier expansions. The shortcomings of the numerical integration is discussed in our recent paper [9]. One of the major reasons is that the process is expensive when simulating many particle, stationary or moving.

ACCEPTED MANUSCRIPT

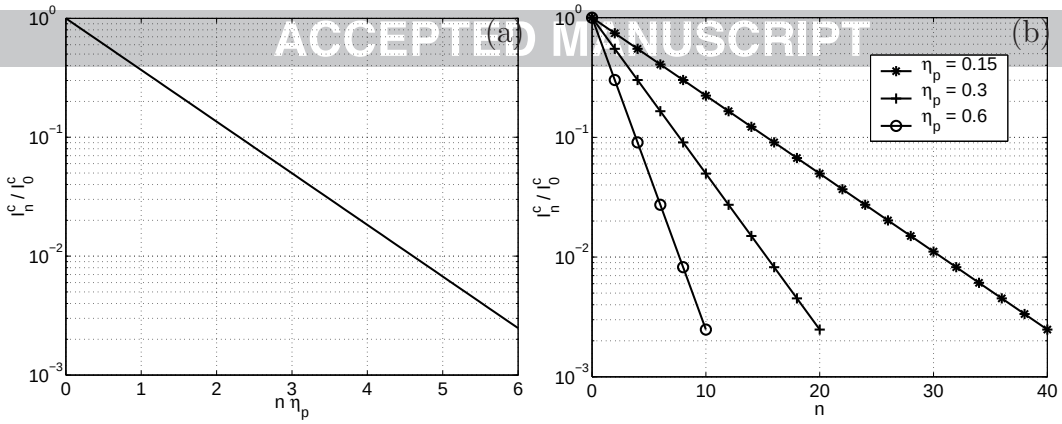

Fig. 5. Normalized non-zero integrations vs.: (a) $n\eta_p$; (b) n for different η_p.

3.5 Algebraic formulas of force and torque

In the rest of this section, we derive the algebraic formulas for the elliptical particle, counterpart of the circular/spherical particle. The results give an efficient approach and also show the underlying physics of the harmonic mode interactions to contribute to the force and torque on particles.

3.5.1 Two basic contour integrations using Residue Theorem

Denote the weight $w = \frac{1}{\sqrt{a-\cos^2\phi}} = \frac{1}{\sqrt{(\sqrt{a}-\cos\phi)(\sqrt{a}+\cos\phi)}}$ with $a = \cosh^2\eta_p > 1$ and $z = \exp(i\phi)$. It can be shown that there are two simple poles $z_1 = -z_2 = \sqrt{a} - \sqrt{a-1}$ for w^2 inside the contour $|z| = 1$. By the contour integration and Residue Theorem, it can be shown that, for $n \geq 0$,

$$\int_0^{2\pi} w^2 \exp(in\phi) d\phi = \pi \frac{[1+(-1)^n]\left(\sqrt{a}-\sqrt{a-1}\right)^n}{\sqrt{a^2-a}} = \pi \frac{[1+(-1)^n]}{\sqrt{a^2-a}\left(\sqrt{a}+\sqrt{a-1}\right)^n} \quad (29)$$

Taking the real and imaginary parts of both sides of the equation yields

$$I_n^c = \int_0^{2\pi} w^2 \cos(n\phi) d\phi = \pi \frac{[1+(-1)^n]}{\sqrt{a^2-a}\left(\sqrt{a}+\sqrt{a-1}\right)^n}, \; I_n^s = \int_0^{2\pi} w^2 \sin(n\phi) d\phi = 0 \quad (30)$$

The derivation is kindly provided by Prof. Prosperetti. We also include an alternative derivation in Sec. D and verify the formulas numerically. The only non-zero integration (for even n in the cosine function) can be normalized

$$I_n^c / I_0^c = \left(\sqrt{a}+\sqrt{a-1}\right)^{-n} = \exp(-n\eta_p), \; I_0^c = 4\pi / \sinh 2\eta_p. \quad (31)$$

ACCEPTED MANUSCRIPT

The normalized integration is shown in Fig. 5(a) in term of $n\eta_p$ and Fig. 5(b) in term of n for different η_p values. The results show that the non-zero integration is exponentially decreased with respect to n, η_p, and their product. The results also show that the integration is non-negligible only when the product of n and η_p is sufficiently small. For a fixed η_p value, the integration is non-negligible only when the mode n is sufficiently low.

3.5.2 Interactions in weighted Fourier basis

To investigate the underlying physics of the mode interactions for the force and torque on the particle, we consider the interactions of the weighted Fourier basis, which is different from the orthogonality relation of the Fourier basis in Sec. A. For the weighted Fourier basis

$$w(1, \cos\phi, \sin\phi, \cos 2\phi, \sin 2\phi, \cdots, \cos n\phi, \sin n\phi, \cdots), \tag{32}$$

it can be shown for the integers $n \geq 0$, $n' \geq 0$, with the help of the two basic contour integrations,

$$\begin{aligned}
&\int_0^{2\pi} w^2 \sin n\phi \cos n'\phi d\phi = \int_0^{2\pi} w^2 \sin n\phi d\phi = 0, \int_0^{2\pi} w^2 \cos n\phi d\phi = I_0^c \exp(-n\eta_p), \\
&\int_0^{2\pi} w^2 \cos n\phi \cos n'\phi d\phi = \frac{I_0^c}{2}[\exp(-|n'-n|\eta_p) + \exp(-(n'+n)\eta_p)], \\
&\int_0^{2\pi} w^2 \sin n\phi \sin n'\phi d\phi = \frac{I_0^c}{2}\left[\exp(-|n'-n|\eta_p) - \exp(-(n'+n)\eta_p)\right],
\end{aligned} \tag{33}$$

which implies that each of the modes interacts with all other modes in addition to itself. However, owing to the exponential decaying as indicated in Fig. 5(a) and (b), each of the modes interacts essentially only with its adjacent modes in addition to itself. This is in contrast to the orthogonality relation of the Fourier modes, each of them interacting with itself.

3.5.3 Difference between circular and elliptical particles

The above extra interactions between the mode and its adjacent modes result in different underlying physics which contributes to the force and toque on the particle. The torque on a conductor particle is non-zero and the torque on a dielectric particle can be non-zero even when uncharged. The force is contributed from all of the interactions including the interactions of the mode with itself and with its adjacent modes as well. Therefore, the interactions are

ACCEPTED MANUSCRIPT

Table 1
Parameters used in the exact solutions of the test cases

Case	AR	η_p	$1/d$	Ω_p	media	Source (0 if unspecified)	Eqs.
I	2	0.55	12	0	conductor	$V^e = 1$	(18) & (21)
II				0.2π	dielectric	$\sigma_n = 10^{-2}$, $n \leq 1$	(16) & (19)
III	10	0.1	20	0.4π	dielectric	$\sigma_n = 1$, $n \leq 1$	(16) & (19)
IV				0.6π	dielectric	$\sigma_n = 10^2$, $n \leq 1$	(16) & (19)
V	50	0.02	90	0.8π	conductor		(17) & (20)
VI	100	0.01	140	$\pi/4$	dielectric		(16) & (19)

more complicated in the elliptical particles than those in the circular particles. However, this complication creats more interesting physical phenomena for the elliptical particles such as alignment and orientation behavior.

4 Numerical results

In our recent papers [8,9], we extensively investigated the performance of the Physalis method for circular/spherical particles: the second-order accuracy; accurate solutions for strong mutual particle-field, particle-particle, and particle-boundary interactions; the efficiency of simulations of particles of the order one hundred thousand and one million using a PC; and simulations of uncharged/charged dielectric/conductor particles, strong jump interface conditions. As expected, these features are retained for the elliptic particles.

For the low aspect ratio (AR of order 1), the ratio of the major and minor semi-axes $a_p \cosh \eta_p / a_p \sinh \eta_p$, the numerical results are similar to those for circular/spherical particles as expected. In the present paper, we focus on cases of high AR. These problems of elongated rod-like particles are very challenging for any numerical method. Note that on the tips of these elongated particles, the electric field is much stronger than other regions due to the much smaller characteristic length scale on the tips. The extreme case is a flat plate, i.e. $\eta_p = 0$, for which it is well-known the existence of the singularity on the tips.

4.1 Test cases

As given in Sec. 2.3, there are many analytical solutions for simple or complex fields when there is only one particle in the electric field. These artificial exact solutions can be used to test the accuracy of the method. Table 1 lists the details of test Case I to VI for the dielectric and conductor with the mode

ACCEPTED MANUSCRIPT

Table 2
Coefficients a_n, b_n calculated in the numerical solutions

AR	2		10		50	100
Case	I	II	III	IV	V	VI
b_0	0.9908	0.9954	0.9977	0.9851	0.9555	0.9852
a_1	0.9902	0.9991	1.0007	1.0007	1.0201	0.9948
b_1	0.9891	0.9963	0.9987	0.9781	0.9994	1.0000
a_2	0.9994	0.9991	0.9999	1.0019	0.9874	0.9996
b_2	0.9985	0.9994	0.9998	0.9860	0.9992	1.0000
a_3	0.9996	0.9983	0.9996	1.0025	1.0021	1.0026
b_3	0.9970	0.9988	0.9996	0.9934	0.9998	1.0000

coefficients $a_n = b_n = 1$ and corresponding space step d. The unspecified coefficients in the source terms are set to zero. These test cases include the AR as low as 2 and as high as 100, different angle Ω_p formed between the major axis and the positive x axis, difference media, and different surface free charge density. In the following discussions, we verify that the Physalis method generates very accurate numerical results and the coefficients can be calculated accurately.

In the following numerical simulations, the Dirichlet boundary conditions are given from the above analytical solutions. The initial guess for the electric field has zero values everywhere. The parameters are $\epsilon^o = 1.0, \epsilon^i = 5.0, a_p = 1.0$, and $N_c = 3$. The corresponding mode coefficients from the numerical simulations are shown in Table 2.

4.2 Low Aspect Ratio

In Case I and II, the AR is as low as 2. The source is also weak, i.e., the jump value σ_n and the specified voltage V^e are comparable to or less than the coefficients a_n and b_n. By comparing the numerical values with the exact values $a_n = b_n = 1$, the relative errors of most of the coefficients are around 0.1%. Therefore, the exact solutions are almost recovered exactly in the Physalis method and the coefficients are numerically predicted very accurate. This fact make it possible to accurately calculate the derivative quantities, such as the local charge distribution, force and torque on the particles.

ACCEPTED MANUSCRIPT

In Case III to VI, the AR is from 10 up to 100. In addition, the strong jump value is investigated. To our knowledge, these challenging problems of elongated rod-like particles with so high an aspect ratio have not yet been reported in the literature. In other numerical methods, an extremely fine mesh has to be used to resolve the geometry of the particle, making the simulation prohibitively expensive. However, in all of these cases, the relative errors of most of the coefficients are around 0.2%. Therefore, as the cases of low AR, the exact solutions are almost recovered exactly and the coefficients are numerically predicted very accurate. As indicated in Table 1, the requirement is that the mesh is sufficiently to resolve the structure of the minor semi-axis but much coarser than other numerical methods.

4.4 Field of the Numerical Error

In Fig. 6, the numerical errors for the representative test cases are shown, where the dotted lines represent the interface between the particle and the outer media. These cases include low aspect ratio, high aspect ration, weak source, strong source, different angle Ω_p, isolated conductor, conductor with specified voltage, and dielectric. In the left hand column, we show the exact solutions which are typically complicated with strong gradients. In the right column, the corresponding numerical errors are shown. In general, the numerical solutions are very accurate. For the case with a low aspect ratio, the numerical solution is similar to those for the circular/spherical particles. The numerical errors occur close to the interface. In contrast, for the case with a high aspect ratio, the numerical errors shrink to the tips of the particle. This is what expected, because the electric field around the tip is much stronger than the rest region.

In addition, the numerical results show that compared with those outside of the particles, the errors inside the particles are negligible. This implies that the closed form of the analytical solutions is almost recovered, consistent with the accurately calculated coefficients in Table 1. The accuracy attributes to the fact that the spectral analytical solution obeys the governing equation and satisfies the interface condition exactly, with convergent coefficients solved through the least square approach. This also indicates that the coefficients in the spectral analytical solution are solved to be more accurate than the global error dominated by that outside of the particle. This feature is important, because the derivative quantities of interest such as surface charge distribution and force/torque on the particles are analytical functions of the solved coefficients and thus have the same accuracy.

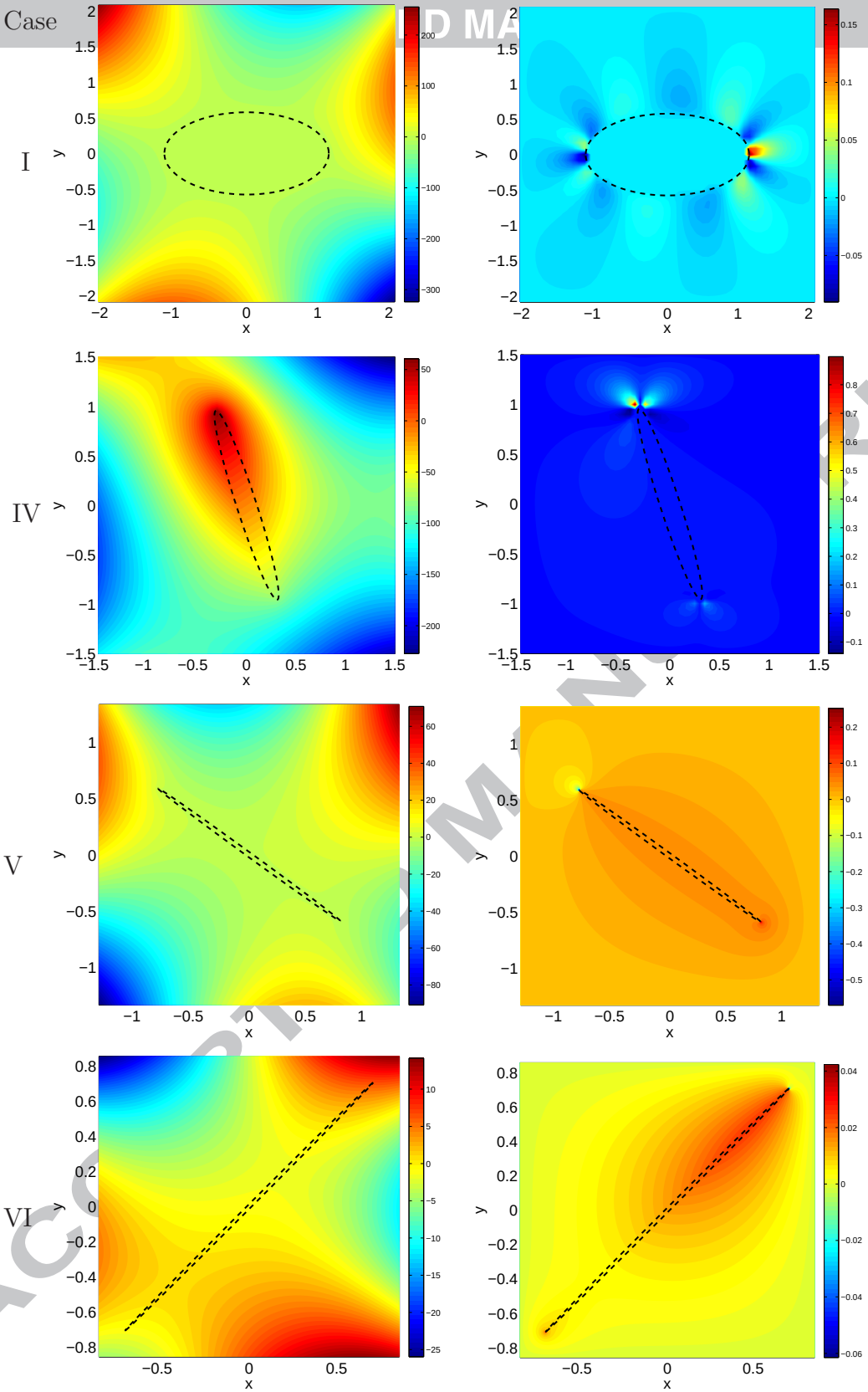

Fig. 6. Left hand column: exact solutions; right hand column: numerical errors.

ACCEPTED MANUSCRIPT

With the above accurate results, it is expected that the method yields accurate numerical results for the interactions between the elliptical particle, field, and boundary, which, to our knowledge, have not yet been reported in the literature. The particle interactions are crucial to the theory of particle chain formation and many applications. However, as indicated in the monograph [10], no model of the elliptic particle chain exists in the literature. Our direct resolution of the elliptic particles make the accurate prediction of the elliptic particle chain possible. In the present paper, we directly resolve the elliptic particles and exactly calculate the force and torque for the first time. The interactions between field, particle, and boundary need to be extensively investigated and will be reported in the subsequent papers.

5 Conclusion and future work

The Physalis method is extended to directly resolve elliptical particles in the electric field and to investigate the mutual fluid-particle, particle-particle, and particle-boundary interactions. The method is numerically verified to be accurate in various situations, including very challenging problems, for example, elongated rod-like particle with very high aspect ratios, which is very challenging for any numerical method. To our knowledge, that problem has not been investigated in other methods accurately.

The accurate simulations of the interactions for elliptical particles are crucial to the theory of particle chain formation and many applications. However, as indicated in the monograph [10], no model of the elliptic particle chain exists in the literature. Our direct resolution of the elliptic particles makes the accurate prediction of the elliptic particle chain possible.

In addition, a long-standing important problem, involving the local charge distribution, DEP force, and torque on the elliptical particle, is solved for the first time. The force and torque on finite-sized particles are rigourously derived with significance in theory and numerical methods. The results are different from those for the circular and spherical particles due to extra interactions between harmonics. Therefore, the interactions are more complicated for the elliptical particles than those in the circular particles. However, this complication creates more interesting physical phenomena for the elliptical particles such as alignment and orientation behavior.

The singularity of the elliptic coordinates are discussed, which is essential to avoid nonphysical solutions of Laplace's equation. Unfortunately, to our

ACCEPTED MANUSCRIPT

knowledge, the singularity has not been discussed in the literature, because interests in other physical problems are mainly for solutions outside of the particles. The anisotropy effects on the local charge distribution and electric field are also discussed.

For the first time, the method directly resolves the elliptical particles with accurate local charge distribution, force, and torque on the particles, making many applications in engineering, mechanics, physics, chemistry, and biology possible. Applications to heterogeneous materials, heterogeneous functional materials, microfluidics, and electric double layer capacitors will be investigated in future work.

The conceptual design and specific engineering of heterogeneous materials requires a capability to resolve and model local details, including the interfaces between phases which control the interaction of the constituents [89,90]. Resolving the boundary conditions precisely, with a minimum of restrictions on the number and proximity of phases is essential to this endeavor. Future work will apply this method to several classes of these problems, including the design of electrodes for fuel cells and batteries, and the dielectric design of materials for managing EMF (electromotive force) intrusions on electrical and structural devices. A special case to be examined is the simulation of observed local three dimensional morphology by assemblies of particles which are sized and packed to simulate observed porosity at the nano- or micro-scale, and arranged as groups to simulate local morphology having larger length scales.

From the numerical perspective, future work includes the extensions to 3D particles [87,91], implementation in locally refined meshes for further efficiency [92], implementation in a parallel code, extension to time-varying problems to model mixtures of real dielectrics with polarization and conduction as well [93], extensions to multiphysical problems, etc.

ACCEPTED MANUSCRIPT

Acknowledgements

The first author (QL) is deeply indebted to his advisors Prof. Kenneth Reifsnider, NAE, and Prof. Andrea Prosperetti, NAE, for invaluable advice. He also would like to thank Prof. Prosperetti for permitting the use of his elegant derivations of the contour integrations in the paper. The present research was supported by the Department of Energy under funding for an EFRC (the HeteroFoaM Center), grant no. DE-SC0001061.

ACCEPTED MANUSCRIPT

A Some properties of Fourier series

The orthogonality relation for the complete basis of the Fourier series is

$$\int_0^{2\pi} \sin n\phi \cos n'\phi d\phi = \int_0^{2\pi} \sin n\phi d\phi = \int_0^{2\pi} \cos n\phi d\phi = 0,$$
$$\int_0^{2\pi} 1 \cdot 1 d\phi = 2\pi, \int_0^{2\pi} \cos n\phi \cos n'\phi d\phi = \int_0^{2\pi} \sin n\phi \sin n'\phi d\phi = \pi\delta_{nn'}, \quad \text{(A.1)}$$

where the integers $n \geq 1$, $n' \geq 1$, and $\delta_{nn'}$ is the Kronecker delta function. The orthogonality relation of the sine and cosine functions yields the Fourier series of an arbitrary function $f(\phi)$:

$$f(\phi) = f_0 + \sum_{n=1}^{\infty} f_n^c \cos n\phi + f_n^s \sin n\phi, \quad \text{(A.2)}$$

where the coefficients

$$f_0 = \frac{1}{2\pi}\int_0^{2\pi} f(\phi)d\phi, \; f_n^c = \frac{1}{\pi}\int_0^{2\pi} \cos n\phi f(\phi)d\phi, \; f_n^s = \frac{1}{\pi}\int_0^{2\pi} \sin n\phi f(\phi)d\phi \quad \text{(A.3)}$$

Consider the integration of the product of two arbitrary functions f and g, where

$$g(\phi) = g_0 + \sum_{n=1}^{\infty} 2n \left(g_n^c \cos n\phi + g_n^s \sin n\phi\right). \quad \text{(A.4)}$$

By the orthogonality relation,

$$\frac{1}{\pi}\int_0^{2\pi} g(\phi)f(\phi)d\phi = 2f_0g_0 + \sum_{n=1}^{\infty} 2n(f_n^c g_n^c + f_n^s g_n^s). \quad \text{(A.5)}$$

B General solution for elliptical particles

Owing to the periodic condition $V(\eta, \phi) = V(\eta, \phi + 2\pi)$ in the elliptic coordinate, the general solution of Laplace's equation can be written as Eq. (13) by separation of variables. It should be stressed that the form can represent

ACCEPTED MANUSCRIPT

any solution, simple or complex. The form of the general solution is valid inside and outside of the particles. The general solution outside of the particle becomes

$$V^o = a_0\eta + b_0 + \sum_{n=1}^{\infty}(a_n e^{n\eta} + c_n e^{-n\eta})\cos n\phi + (b_n e^{n\eta} + d_n e^{-n\eta})\sin n\phi, \quad \text{(B.1)}$$

B.1 General solution for dielectrics

Inside the particle, the constrain Eq. (14) reduces Eq. (13) to

$$V^i = b_0^i + \sum_{n=1}^{\infty} a_n^i(e^{n\eta} + e^{-n\eta})\cos n\phi + b_n^i(e^{n\eta} - e^{-n\eta})\sin n\phi. \quad \text{(B.2)}$$

Owing to the orthogonality relation, the interface condition Eq. (1) yields

$$\begin{cases} a_0 = -\frac{\sigma_0}{\epsilon^o},\ b_0^i = b_0 - \frac{\sigma_0}{\epsilon^0}\eta_p \\ a_n^i = \frac{2\epsilon^o e^{n\eta_p} a_n + \sigma_n^c/n}{(\epsilon^o+\epsilon^i)e^{n\eta_p} + (\epsilon^o-\epsilon^i)e^{-n\eta_p}},\ c_n^o = \frac{[(\epsilon^o-\epsilon^i)e^{3n\eta_p} + (\epsilon^o+\epsilon^i)e^{n\eta_p}]a_n + (e^{2n\eta_p}+1)\sigma_n^c/n}{(\epsilon^o+\epsilon^i)e^{n\eta_p} + (\epsilon^o-\epsilon^i)e^{-n\eta_p}} \\ b_n^i = \frac{2\epsilon^o e^{n\eta_p} b_n + \sigma_n^s/n}{(\epsilon^i+\epsilon^o)e^{n\eta_p} + (\epsilon^i-\epsilon^o)e^{-n\eta_p}},\ d_n^o = \frac{[(\epsilon^o-\epsilon^i)e^{3n\eta_p} - (\epsilon^o+\epsilon^i)e^{n\eta_p}]b_n + (e^{2n\eta_p}-1)\sigma_n^s/n}{(\epsilon^i+\epsilon^o)e^{n\eta_p} + (\epsilon^i-\epsilon^o)e^{-n\eta_p}}. \end{cases} \quad \text{(B.3)}$$

By plugging the solved coefficients into Eqs. (B.1)-(B.2), the general solutions for the dielectric particle Eqs. (16) and (19) are obtained.

B.2 General solution for conductors

For conductor particles, the potential is a constant inside the particle, i.e., $0 \le \eta \le \eta_p$. Thus, Eq. (13) reduces to the general solutions inside conductor particles:

$$V^i = b_0^i. \quad \text{(B.4)}$$

Owing to the orthogonality, the interface conditions for isolated conductor particle yields

$$a_0 = -\frac{Q}{2\pi\epsilon^o},\ b_0^i = -\frac{Q}{2\pi\epsilon^o}\eta_p + b_0,\ c_n = -e^{2n\eta_p}a_n,\ d_n = -e^{2n\eta_p}b_n, \quad \text{(B.5)}$$

ACCEPTED MANUSCRIPT

and the general solutions for the isolated conductor particle Eqs. (17) and (20) are obtained. Similarly, the interface condition of an imposed voltage yields:

$$b_0^i = V^e,\ b_0 = V^e - a_0\eta_p,\ c_n = -e^{2n\eta_p}a_n,\ d_n = -e^{2n\eta_p}b_n, \tag{B.6}$$

and the general solutions Eqs. (18) and (21) are obtained for which the unknown coefficient notation a_0 is replaced by b_0 so that, for all of the cases, the formulas have the same set of unknowns a_n and b_n.

C Relations for calculating force and torque on elliptical particles

Some relations are given in this section for the derivations of the force and torque on the elliptical particles. We denote $\mathcal{Y}_n^{c+} = e^{n\eta}\cos n\phi$, $\mathcal{Y}_n^{s+} = e^{n\eta}\sin n\phi$, $\mathcal{Z}_n^{c-} = e^{-n\eta}\cos n\phi$, and $\mathcal{Y}_n^{s-} = e^{-n\eta}\sin n\phi$ for convenience and derive their derivatives and cross products related to their gradients. The partial derivative operators are

$$\frac{h^2}{a_p}\frac{\partial}{\partial x} = \sinh\eta\cos\phi\frac{\partial}{\partial\eta} - \cosh\eta\sin\phi\frac{\partial}{\partial\phi},\ \frac{h^2}{a_p}\frac{\partial}{\partial y} = \cosh\eta\sin\phi\frac{\partial}{\partial\eta} + \sinh\eta\cos\phi\frac{\partial}{\partial\phi} \tag{C.1}$$

$$\vec{r}\times(-\nabla) = -\hat{z}\frac{a_p^2}{h^2}\left(\sin\phi\cos\phi\frac{\partial}{\partial\eta} + \sinh\eta\cosh\eta\frac{\partial}{\partial\phi}\right). \tag{C.2}$$

The derivatives for the force in the x direction become

$$\frac{\partial\mathcal{Y}_n^{c+}}{\partial x} = \frac{a_p n e^{n\eta}}{2h^2}\left[e^{\eta}\cos(n-1)\phi - e^{-\eta}\cos(n+1)\phi\right], \tag{C.3}$$

$$\frac{\partial\mathcal{Y}_n^{c-}}{\partial x} = \frac{a_p n e^{-n\eta}}{2h^2}\left[-e^{\eta}\cos(n+1)\phi + e^{-\eta}\cos(n-1)\phi\right], \tag{C.4}$$

$$\frac{\partial\mathcal{Y}_n^{s+}}{\partial x} = \frac{a_p n e^{n\eta}}{2h^2}\left[e^{\eta}\sin(n-1)\phi - e^{-\eta}\sin(n+1)\phi\right], \tag{C.5}$$

$$\frac{\partial\mathcal{Y}_n^{s-}}{\partial x} = \frac{a_p n e^{-n\eta}}{2h^2}\left[-e^{\eta}\sin(n+1)\phi + e^{-\eta}\sin(n-1)\phi\right], \tag{C.6}$$

$$\frac{\partial\eta}{\partial x} = \frac{a_p}{2h^2}\left(e^{\eta}\cos\phi - e^{-\eta}\cos\phi\right), \tag{C.7}$$

and in the y direction become

$$\frac{\partial\mathcal{Y}_n^{c+}}{\partial y} = \frac{a_p n e^{n\eta}}{2h^2}\left[-e^{\eta}\sin(n-1)\phi + e^{-\eta}\sin(n+1)\phi\right], \tag{C.8}$$

$$\frac{\partial\mathcal{Y}_n^{c-}}{\partial y} = \frac{a_p n e^{-n\eta}}{2h^2}\left[-e^{\eta}\sin(n+1)\phi + e^{-\eta}\sin(n-1)\phi\right], \tag{C.9}$$

ACCEPTED MANUSCRIPT

$$\frac{\partial \mathcal{Y}_n^{s+}}{\partial y} = \frac{a_p n e^{n\eta}}{2h^2}\left[e^{\eta}\cos(n-1)\phi - e^{-\eta}\cos(n+1)\phi\right], \tag{C.10}$$

$$\frac{\partial \mathcal{Y}_n^{s-}}{\partial y} = \frac{a_p n e^{-n\eta}}{2h^2}\left[e^{\eta}\cos(n+1)\phi - e^{-\eta}\cos(n-1)\phi\right], \tag{C.11}$$

$$\frac{\partial \eta}{\partial y} = \frac{a_p}{2h^2}\left(e^{\eta}\sin\phi + e^{-\eta}\sin\phi\right). \tag{C.12}$$

The cross products for the torque become

$$\vec{r}\times(-\nabla\mathcal{Y}_n^{c+}) = \frac{a_p^2 n e^{n\eta}}{4h^2}\left[-\sin(n+2)\phi + \sin(n-2)\phi + (e^{2\eta}-e^{-2\eta})\sin n\phi\right],$$

$$\vec{r}\times(-\nabla\mathcal{Y}_n^{c-}) = \frac{a_p^2 n e^{-n\eta}}{4h^2}\left[\sin(n+2)\phi - \sin(n-2)\phi + (e^{2\eta}-e^{-2\eta})\sin n\phi\right],$$

$$\vec{r}\times(-\nabla\mathcal{Y}_n^{s+}) = -\frac{a_p^2 n e^{n\eta}}{4h^2}\left[\cos(n-2)\phi - \cos(n+2)\phi + (e^{2\eta}-e^{-2\eta})\cos n\phi\right],$$

$$\vec{r}\times(-\nabla\mathcal{Y}_n^{s-}) = -\frac{a_p^2 n e^{-n\eta}}{4h^2}\left[-\cos(n-2)\phi + \cos(n+2)\phi + (e^{2\eta}-e^{-2\eta})\cos n\phi\right],$$

$$\vec{r}\times(-\nabla\eta) = -\frac{a_p^2}{2h^2}\sin 2\phi.$$

The second order differential operators in Laplace's equation can be written as

$$\begin{aligned} h^2\frac{\partial^2}{\partial x^2} &= \sinh\eta\cosh\eta\left(1-2\cos^2\phi\frac{\sinh^2\eta-\sin^2\phi}{\cosh^2\eta-\cos^2\phi}\right)\frac{\partial}{\partial\eta} + \sinh^2\eta\cos^2\phi\frac{\partial^2}{\partial\eta^2} \\ &\quad + \sin\phi\cos\phi\left(1+2\cosh^2\eta\frac{\sinh^2\eta-\sin^2\phi}{\cosh^2\eta-\cos^2\phi}\right)\frac{\partial}{\partial\phi} + \cosh^2\eta\sin^2\phi\frac{\partial^2}{\partial\phi^2} \\ &\quad - 2\sinh\eta\cosh\eta\sin\phi\cos\phi\frac{\partial^2}{\partial\eta\partial\phi}, \end{aligned} \tag{C.13}$$

$$\begin{aligned} h^2\frac{\partial^2}{\partial y^2} &= \sinh\eta\cosh\eta\left(1-2\sin^2\phi\frac{\cosh^2\eta+\cos^2\phi}{\cosh^2\eta-\cos^2\phi}\right)\frac{\partial}{\partial\eta} + \cosh^2\eta\sin^2\phi\frac{\partial^2}{\partial\eta^2} \\ &\quad + \sin\phi\cos\phi\left(1-2\sinh^2\eta\frac{\cosh^2\eta+\cos^2\phi}{\cosh^2\eta-\cos^2\phi}\right)\frac{\partial}{\partial\phi} + \sinh^2\eta\cos^2\phi\frac{\partial^2}{\partial\phi^2} \end{aligned} \tag{C.14}$$

D Alternative derivation of two basic contour integrations

Since $z = \exp(i\phi)$, we have

$$\cos n\phi = \frac{1}{2}(z^n + z^{-n}),\ \sin n\phi = \frac{1}{2i}(z^n - z^{-n}),\ d\phi = \frac{1}{iz}dz. \tag{D.1}$$

ACCEPTED MANUSCRIPT

Plugging the relations to the integrations, we have

$$I_n^s = \int_0^{2\pi} w^2 \sin(n\phi) d\phi = -2(I^+ - I^-),\ I_n^c = \int_0^{2\pi} w^2 \cos(n\phi) d\phi = 2i(I^+ + I^-) \quad \text{(D.2)}$$

where

$$I^+ = \int_0^{2\pi} \frac{z^{2n+1}}{z^4 - (4a-2)z^2 + 1} dz,\ I^- = \int_0^{2\pi} \frac{1}{z^{n-1}[z^4 - (4a-2)z^2 + 1]} dz \quad \text{(D.3)}$$

Note that there is a pole $z = 0$ with the order $n - 1$ in I^-. The residue could be found using the differential operator of $n - 2$ or the combined Taylor and Laurent series. Instead, we can avoid the high order poles as follows.

For the periodic functions, $\int_0^{2\pi} = \int_\alpha^{\alpha+2\pi}$. Since w^2 is an even function and $\sin n\phi$ is an odd function, the integration $I_n^s = 0$, yielding $I^- = I^+$ which is actually already found in Sec. 3.5.1. Therefore, we find the value of I_n^c and, in addition, the integration of high order pole is also found. Note that, in this approach, taking $I_n^c + iI_n^s$ and taking the real and imaginary parts of the contour integration recover the approach in Sec. 3.5.1.

E Surface charge, force, and torque on circular particles

The local surface charge distribution, force, and torque on the circular conductor/dielectric particles are given in this section. The key to calculate the force and torque is to utilize the orthogonality relation. The derivations are similar to those in our recent paper [9] for three dimensions.

E.1 Relations for calculating force and torque

Some relations are given for the derivations of the force and torque. The goal is to rewrite the compound expressions to the linear combinations of the trigonometric functions so that the integration of the product of two functions, Eq. (A.5), can be easily obtained. We denote $\mathcal{Z}_n^{c+} = r^n \cos n\phi$, $\mathcal{Z}_n^{s+} = r^n \sin n\phi$, $\mathcal{Z}_n^{c-} = r^{-n} \cos n\phi$, and $\mathcal{Z}_n^{s-} = r^{-n} \sin n\phi$ for convenience and derive their derivatives and cross products related to their gradients. The partial derivative operators are

ACCEPTED MANUSCRIPT

$$\frac{\partial}{\partial x}=\cos\phi\frac{\partial}{\partial r}-\frac{\sin\phi}{r}\frac{\partial}{\partial\phi},\ \frac{\partial}{\partial y}=\sin\phi\frac{\partial}{\partial r}+\frac{\cos\phi}{r}\frac{\partial}{\partial\phi},\ \vec{r}\times(-\nabla)=-\hat{z}\frac{\partial}{\partial\phi}.$$

The derivatives for the force in the x and y directions become

$$\begin{aligned}
r^{-n+1}\frac{\partial\mathcal{Z}_n^{c+}}{\partial x}&=n\cos(n-1)\phi,\ r^{n+1}\frac{\partial\mathcal{Z}_n^{c-}}{\partial x}=-n\cos(n+1)\phi,\\
r^{-n+1}\frac{\partial\mathcal{Z}_n^{S+}}{\partial x}&=n\sin(n-1)\phi,\ r^{n+1}\frac{\partial\mathcal{Z}_n^{s-}}{\partial x}=-n\sin(n+1)\phi,\\
r^{-n+1}\frac{\partial\mathcal{Z}_n^{c+}}{\partial y}&=-n\sin(n-1)\phi,\ r^{n+1}\frac{\partial\mathcal{Z}_n^{c-}}{\partial y}=-n\sin(n+1)\phi,\\
r^{-n+1}\frac{\partial\mathcal{Z}_n^{S+}}{\partial y}&=n\cos(n-1)\phi,\ r^{n+1}\frac{\partial\mathcal{Z}_n^{s-}}{\partial y}=n\cos(n+1)\phi,\\
r\frac{\partial\ln r}{\partial x}&=\cos\phi,\ r\frac{\partial\ln r}{\partial y}=\sin\phi.
\end{aligned}$$

For any integer k, the cross products for the torque become

$$\begin{aligned}
r^{-k}\vec{r}\times(-\nabla r^k\cos n\phi)&=n\sin n\phi\hat{z},\ r^{-k}\vec{r}\times(-\nabla r^k\sin n\phi)=-n\cos n\phi\hat{z},\\
\vec{r}\times(-\nabla\ln r)&=0.
\end{aligned}$$

E.2 General case

For convenience, we generalize the dielectric and conductor cases to the following with the potential outside the particle

$$\begin{aligned}
V^o=&a_0^+ +\sum_{n=1}^{\infty}r_p^{-n+1}r^n\left(a_n^+\cos n\phi+b_n^+\sin n\phi\right)\\
&+r_pa_0^-\ln r+\sum_{n=1}^{\infty}r_p^{n+1}r^{-n}\left(a_n^-\cos n\phi+b_n^-\sin n\phi\right),
\end{aligned}\tag{E.1}$$

where $a_n^{+,-}$ and $b_n^{+,-}$ are the coefficients of the modes $\cos n\phi$ and $\sin n\phi$, respectively, and the subscript $+$ is for the nonnegative exponent r^n while $-$ is for the negative exponent r^{-n} or $\ln r$. It can be shown that the components of the electric field intensity $\vec{E}^o=-\nabla V^o$ at $r=r_p$

$$\begin{aligned}
E_x=&-a_1^+-(a_0^-+2a_2^+)\cos\phi-2b_2^+\sin\phi\\
&-\sum_{n=2}^{\infty}\left[(n+1)a_{n+1}^+-(n-1)a_{n-1}^-\right]\cos n\phi+\left[(n+1)b_{n+1}^+-(n-1)b_{n-1}^-\right]\sin n\phi,\\
E_y=&-b_1^+-(a_0^--2a_2^+)\sin\phi-2b_2^+\cos\phi
\end{aligned}$$

ACCEPTED MANUSCRIPT

$$-\sum_{n=2}^{\infty} -\left[(n+1)a_{n+1}^{+}+(n-1)a_{n-1}^{-}\right]\sin n\phi+\left[(n+1)b_{n+1}^{+}+(n-1)b_{n-1}^{-}\right]\cos n\phi \tag{E.2}$$

The surface charge density at $r = r_p$ is supposed to be

$$\frac{\sigma_t}{(\epsilon^o)^\nu} = -a_0^- + \sum_{n=1}^{\infty} 2n\left(a_n^- \cos n\phi + b_n^- \sin n\phi\right), \tag{E.3}$$

where the coefficients a_n^- and b_n^- are the same as those for the negative exponents in V^o, and ν is a parameter (In the following results, $\nu = 1$ for a conductor while $\nu = 0$ for a dielectric particle). Note that in the general case, these coefficients are independent to each other and the interactions between the harmonic modes can be clearly seen. However, the coefficients a_n^+ and a_n^- are closely related to each other as b_n^+ and b_n^- are in the dielectric and conductor particles discussed following the general case.

Eq. (6) gives the normalized force

$$\vec{F}^* = \frac{\vec{F}}{2\pi\gamma(\epsilon^o)^{1+\nu}r_p} = \frac{1}{2\pi}\int_0^{2\pi} d\phi \frac{\sigma_t}{(\epsilon^o)^\nu}(E_x\hat{x}+E_y\hat{y}). \tag{E.4}$$

Given the Fourier expansions of the electric field intensity in Eq. (E.2) and the surface charge density in Eq. (E.3), it is straightforward to calculate the surface integration, by using the formula for the integration of the product of two functions in Sec. A. The force reduces to

$$\begin{aligned}
F_x^* =& a_1^+ a_0^- - (a_0^- + 2a_2^+)a_1^- - 2b_2^+ b_1^- \\
&- \sum_{n=2}^{\infty} n\left[(n+1)a_{n+1}^+ - (n-1)a_{n-1}^-\right]a_n^- + n\left[(n+1)b_{n+1}^+ - (n-1)b_{n-1}^-\right]b_n^-, \\
F_y^* =& b_1^+ a_0^- - (a_0^- - 2a_2^+)b_1^- - 2b_2^+ a_1^- \\
&- \sum_{n=2}^{\infty} -n\left[(n+1)a_{n+1}^+ + (n-1)a_{n-1}^-\right]b_n^- + n\left[(n+1)b_{n+1}^+ + (n-1)b_{n-1}^-\right]a_n^-
\end{aligned} \tag{E.5}$$

with intermediate steps omitted for brevity.

Eq. (6) gives the normalized torque

$$\vec{T}^* = \frac{\vec{T}}{2\pi\gamma(\epsilon^o)^{1+\nu}r_p^2} = \frac{1}{2\pi}\int_0^{2\pi} d\phi \frac{\sigma_t}{(\epsilon^o)^\nu} L_z\hat{z} \tag{E.6}$$

where $\vec{L} = \hat{r}\times(-\nabla V^o)$, whose component can be written as

ACCEPTED MANUSCRIPT

$$L_z = \sum_{n=1}^{\infty} n\left(a_n^+ \sin n\phi - b_n^+ \cos n\phi\right) + n\left(a_n^- \sin n\phi - b_n^- \cos n\phi\right).$$

Given the Fourier expansions of $\vec{L}$ and the surface charge density in Eq. (E.3), similar to the force, the components of the torque reduce to

$$T_z^* = \sum_{n=1}^{\infty} n^2\left(a_n^+ b_n^- - b_n^+ a_n^-\right). \tag{E.7}$$

It is clear that both the force and the torque are resulted from the interactions between the adjacent harmonic modes, which implies that the resultant force is zero if there is only one mode.

E.3 Conductor

The general solution of the potential outside of the isolated conductor particle is given by

$$V^o = -\frac{Q}{2\pi\epsilon^o}\ln r + b_0 + \sum_{n=1}^{\infty}\left[1 - \left(\frac{r_p}{r}\right)^{2n}\right] r^n(a_n \cos n\phi + b_n \sin n\phi), \tag{E.8}$$

from which the total surface charge density in Eq. (5) reduces to

$$\frac{\sigma_t}{\epsilon^o} = \frac{Q}{2\pi\epsilon^o r_p} - \sum_{n=1}^{\infty} 2n r_p^{n-1}(a_n \cos n\phi + b_n \sin n\phi). \tag{E.9}$$

Comparing them with Eqs. (E.1) and (E.3) in the general case, the corresponding coefficients are

$$a_n^+ = r_p^{n-1} a_n,\ b_n^+ = r_p^{n-1} b_n,\ a_0^+ = b_0,\ a_n^- = -a_n^+,\ b_n^- = -b_n^+,\ a_0^- = -\frac{Q}{2\pi\epsilon^o r_p}.$$

Plugging these coefficients into Eq. (E.5) yields the force and into Eq. (E.7) yields the torque. The components of the resultant force and torque become

$$F_x^* = -\frac{Q}{\pi\epsilon^o r_p} a_1 + \sum_{n=1}^{\infty} 2n(n+1) r_p^{2n-1}\left[a_n a_{n+1} + b_n b_{n+1}\right], \tag{E.10}$$

$$F_y^* = -\frac{Q}{\pi\epsilon^o r_p} b_1 + \sum_{n=1}^{\infty} 2n(n+1) r_p^{2n-1}\left[a_n b_{n+1} - b_n a_{n+1}\right], \tag{E.11}$$

ACCEPTED MANUSCRIPT

$$T_z^* = \sum_{n=1}^{\infty} n^2 \left(-a_n^+ b_n^+ + b_n^+ a_n^+\right) = 0. \tag{E.12}$$

The zero resultant torque is consistent with the fact that the local electric field is perpendicular to the particle surface, implying $\hat{r} \times \vec{E}^o = 0$ and thus $\vec{T} = 0$. By inserting $Q = -2\pi\epsilon^o a_0$ into the above formulas, we obtain all results for the case of a conductor with a specific voltage.

E.4 Dielectrics

The surface free charge density can be expressed as the Fourier series:

$$\sigma = \sigma_0 + \sum_{n=1}^{\infty} [\sigma_n^c \cos n\phi + \sigma_n^s \sin n\phi], \tag{E.13}$$

where the coefficients have the form

$$\sigma_0 = \frac{1}{2\pi} \int_0^{2\pi} \sigma(\phi) d\phi, \;\; \sigma_n^c = \frac{1}{\pi} \int_0^{2\pi} \cos n\phi \sigma(\phi) d\phi, \;\; \sigma_n^s = \frac{1}{\pi} \int_0^{2\pi} \sin n\phi \sigma(\phi) d\phi \tag{E.14}$$

The general solutions of the potential outside of and inside the dielectric particle are given by

$$\begin{aligned} V^o = & -\frac{\sigma_0 r_p}{\epsilon^o} \ln r + \sum_{n=1}^{\infty} \frac{r_p}{(\epsilon^o + \epsilon^i)n} \left(\frac{r_p}{r}\right)^n (\sigma_n^c \cos n\phi + \sigma_n^s \sin n\phi) \\ & + b_o + \sum_{n=1}^{\infty} \left[1 + \frac{\epsilon^o - \epsilon^i}{\epsilon^o + \epsilon^i} \left(\frac{r_p}{r}\right)^{2n}\right] r^n (a_n \cos n\phi + b_n \sin n\phi), \end{aligned} \tag{E.15}$$

$$\begin{aligned} V^i = & -\frac{\sigma_0 r_p}{\epsilon_o} \ln r_p + \sum_{n=1}^{\infty} \frac{r_p}{(\epsilon^o + \epsilon^i)n} \left(\frac{r}{r_p}\right)^n (\sigma_n^c \cos n\phi + \sigma_n^s \sin n\phi) \\ & + b_o + \sum_{n=1}^{\infty} \frac{2\epsilon^o}{\epsilon^o + \epsilon^i} r^n (a_n \cos n\phi + b_n \sin n\phi), \end{aligned} \tag{E.16}$$

from which the total surface charge density in Eq. (5) reduces to

$$\sigma_t = \frac{\sigma_0}{\epsilon^o} + \frac{2}{\epsilon^o + \epsilon^i} \sum_{n=1}^{\infty} [\sigma_n^c + n(\epsilon^o - \epsilon^i) r_p^{n-1} a_n] \cos n\phi + [\sigma_n^s + n(\epsilon^o - \epsilon^i) r_p^{n-1} b_n] \sin n\phi \tag{E.17}$$

By denoting the factors $D_n = n(\epsilon^o + \epsilon^i)$ and $N_n = n(\epsilon^o - \epsilon^i)$ and comparing the potential and surface charge density with Eqs. (E.1) and (E.3), the corresponding coefficients are

ACCEPTED MANUSCRIPT

$$a_n^+ = r_p^{n-1} a_n,\ b_n^+ = r_p^{n-1} b_n,\ a_0^+ = b_0, \tag{E.18}$$

$$a_n^- = \frac{N_n a_n^+ + \sigma_n^c}{D_n},\ b_n^- = \frac{N_n b_n^+ + \sigma_n^s}{D_n},\ a_0^- = -\frac{\sigma_0}{\epsilon^o}. \tag{E.19}$$

Plugging these coefficients into Eqs. (E.5) yields the force and into Eqs. (E.7) yields the torque. Since the self contribution of the induced charge should be exactly zero, the products of two $.^-$ terms need to be set to zero. The components of the resultant force and torque are

$$\begin{aligned} F_x^* = &-a_1 \frac{\sigma_0}{\epsilon^o} - \sum_{n=1}^{\infty} n(n+1) r_p^n a_{n+1} (N_n r_p^{n-1} a_n + \sigma_n^c)/D_n \\ &- \sum_{n=1}^{\infty} n(n+1) r_p^n b_{n+1} (N_n r_p^{n-1} b_n + \sigma_n^s)/D_n, \end{aligned} \tag{E.20}$$

$$\begin{aligned} F_y^* = &-b_1 \frac{\sigma_0}{\epsilon^o} - \sum_{n=1}^{\infty} n(n+1) r_p^n b_{n+1} (N_n r_p^{n-1} a_n + \sigma_n^c)/D_n \\ &+ \sum_{n=1}^{\infty} n(n+1) r_p^n a_{n+1} (N_n r_p^{n-1} b_n + \sigma_n^s)/D_n, \end{aligned} \tag{E.21}$$

$$T_z^* = \sum_{n=1}^{\infty} n^2 r_p^{n-1} \left(a_n \sigma_n^s - b_n \sigma_n^c\right)/D_n. \tag{E.22}$$

Note that as $\epsilon^i \gg \epsilon^o$, the formulas reduces to the counterparts for conductors for uncharged particles, confirming the validity of the above formulas.

References

[1] A. Prosperetti, H. N. Oguz, Physalis: A new o(n) method for the numerical simulation of disperse systems: Potential flow of spheres, J. Comput. Phys. 167 (2001) 196–216.

[2] S. Takagi, H. Oguz, Z. Zhang, A. Prosperetti, Physalis: a new method for particle simulation part ii: two-dimensional navierstokes flow around cylinders, J. Comput. Phys. 187 (2003) 371–390.

[3] Z. Zhang, A. Prosperetti, A second-order method for three-dimensional particle simulation, J. Comput. Phys. 210 (2005) 292–324.

[4] Q. Zhang, A. Prosperetti, Pressure-driven flow in a two-dimensional channel with porous walls, J. Fluid Mech. 631 (2009) 1–21.

[5] Q. Liu, A. Prosperetti, Wall effects on a rotating sphere, J. Fluid Mech. 657 (2010) 1–21.

ACCEPTED MANUSCRIPT

[6] A. Naso, A. Prosperetti, Interaction between a solid particle and a turbulent flow, New J. Phys. 12 (2010) 033040.

[7] Q. Liu, A. Prosperetti, Pressure-driven flow in a channel with porous walls, J. Fluid Mech. 679 (2011) 77–100.

[8] Q. Liu, Physalis method for heterogeneous mixtures of dielectrics and conductors: Accurately simulating one million particles using a pc, J. Comput. Phys. 230 (2011) 8256–8274.

[9] Q. Liu, Directly resolving particles in an electric field: local charge, force, torque, and applications, Int. J. Numer. Meth. Engng 90 (2012) 537–568.

[10] T. B. Jones, Electromechanics of particles, Cambridge University Press, Cambridge, England, 2005.

[11] A. Majumdar, C. H. Lin, Gate capacitance of cylindrical nanowires with elliptical cross-sections, Applied Physics Letters 98 (2011) 073506.

[12] J. Huang, R. Qiao, B. G. Sumpter, V. Meunier, Effect of diffuse layer and pore shapes in mesoporous carbon supercapacitors, J. mater. Res. 25 (2010) 1469–1475.

[13] O. A. Stafford, B. R. Hinderliter, S. G. Croll, Electrochemical impedance spectroscopy response of water uptake in organic coatings by finite element methods, Electrochimica Acta 52 (2006) 1339–1348.

[14] B. J. Connolly, J. R. Scully, Transition from localized corrosion to stress corrosion cracking in an al-li-cu-ag alloy, Corrosion 61 (2005) 1145–1166.

[15] K. L. Reifsnider, P. Fazzino, P. K. Majumdar, L. Xing, Material state changes as a basis for prognosis in aeronautical structures, J. Aeronautical Society 113 (2009) 789–798.

[16] P. D. Fazzino, K. L. Reifsnider, P. Majumdar, Impedance spectroscopy for progressive damage analysis in woven composites, Composites Science and Technology 69 (2009) 2008–2014.

[17] K. L. Reifsnider, S. W. Case, Durability and Damage Tolerance of Material Systems, John Wiley & Sons, New York, 2002.

[18] P. D. Fazzino, K. L. Reifsnider, Electrochemical impedance spectroscopy detection of damage in out of plane fatigue fiber reinforced composite materials, Applied Composite Materials 15 (2008) 127–138.

[19] E. Bogatin, D. DeGroot, S. Gupta, Frequency dependent material properties, Proc. DesignCon 2010, Santa Clara, CA.

[20] P. G. Huray, Foundations of Signal Integrity, John Wiley & Sons., Inc., 2010.

[21] M. U. Ozcan, S. Oca, C. Basdogan, G. Dogusoy, Y. Toka, Characterization of frequency-depencent material properties of human liver and its pathologies using an impact hammer, Medical Image Analysis 15 (2011) 45–52.

ACCEPTED MANUSCRIPT

[22] P. Robin, High Speed Heterostructure Devices, Cambridge University Press, 2001.

[23] K. L. Reifsnider, F. Rabbi, R. Raihan, Q. Liu, P. Majumdar, Y. Du, J. M. Adkins, Heterofoam: New concepts and tools for heterogeneous functional material design, Materials Science and Technology (2011) in press.

[24] R. S. Lakes, Size effects and micromechanics of a porous solid, J. Materials Science 18 (1983) 2572–2581.

[25] P. M. Buechner, R. S. Lakes, Size effects in the elasticity and viscoelasticity of bone, Biomechanics and Modeling in Mechanobiology 1 (2003) 295–301.

[26] Z. Suo, X. Zhao, W. H. Greene, A nonlinear field theory of deformable dielectrics, Journal of the Mechanics and Physics of Solids 56 (2008) 467–486.

[27] T. Belytschko, T. Black, Elastic crack growth in finite elements with minimal remeshing, Int. J. Numer. Meth. Engng 45 (1999) 601–620.

[28] N. Moes, M. Dolbow, T. Belytschko, A finite element method for crack growth without remeshing, Int. J. Numer. Meth. Engng 46 (1999) 131–150.

[29] N. Sukumar, N. Moes, B. Moran, T. Belytschko, Extended finite element method for three-dimensional crack modelling, Int. J. Numer. Meth. Engng 48 (2000) 1549–1570.

[30] C. Daux, N. Moes, M. Dolbow, N. Sukumar, T. Belytschko, Arbitrary branched and intersecting cracks with the extended finite element method, Int. J. Numer. Meth. Engng 48 (2000) 1741–1760.

[31] T. Belytschko, N. Moes, S. Usui, Parimi, Arbitrary discontinuities in finite elements, Int. J. Numer. Meth. Engng 50 (2001) 993–1013.

[32] J. Dolbow, I. Harari, An efficient finite element method for embedded interface problems, Int. J. Numer. Meth. Engng 78 (2009) 229–252.

[33] A. Gerstenberger, W. A. Wall, An embedded dirichlet formulation for 3d continua, Int. J. Numer. Meth. Engng 82 (2010) 537–563.

[34] G. Legrain, P. Cartraud, I. Perreard, N. Moes, An x-fem and level set computational approach for image-based modelling: Application to homogenization, Int. J. Numer. Meth. Engng 86 (2011) 915–934.

[35] S. E. Ashari, S. Mohammadi, Delamination analysis of composites by new orthotropic bimaterial extended finite element method, Int. J. Numer. Meth. Engng 86 (2011) 1507–1543.

[36] C. L. Richardson, J. Hegemann, E. Sifakis, J. Hellrung, J. M. Teran, An xfem method for modeling geometrically elaborate crack propagation in brittle materials, Int. J. Numer. Meth. Engng In Press.

[37] T. Strouboulis, I. Babuska, K. Copps, The design and analysis of the generalized finite element method, Comput. Methods Appl. Mech. Engrg. 181 (2000) 43–69.

ACCEPTED MANUSCRIPT

[38] T. Strouboulis, K. Copps, I. Babuska, The generalized finite element method: an example of its implementation and illustration of its performance, Int. J. Numer. Meth. Engng 47 (2000) 1401–1417.

[39] I. Babuska, U. Banerjee, J. E. Osborn, Generalized finite element methods: main ideas, results and perspectives, International Journal of Computer Mathematics 1 (2004) 67–103.

[40] I. Babuska, G. Caloz, J. E. Osborn, Special finite element methods for a class of second order elliptic problems with rough coefficients, SIAM Journal on Numerical Analysis 31 (1994) 945–981.

[41] J. M. Melenk, I. Babuska, The partition of unity finite element method: basic theory and applications, Comput. Methods Appl. Mech. Engrg. 139 (1996) 289–314.

[42] I. Babuska, J. M. Melenk, The partition of unity method, Int. J. Numer. Meth. Engng 40 (1997) 727–758.

[43] M. Griebel, M. A. Schweitzer, A particle-partition of unity method for the solution of elliptic, parabolic and hyperbolic pdes, SIAM Journal on Scientific Computing 22 (2000) 853–890.

[44] C. Farhat, I. Harari, L. P. Franca, The discontinuous enrichment method, Comput. Methods Appl. Mech. Engrg. 190 (2001) 6455–6479.

[45] C. Farhat, I. Harari, U. Hetmaniuk, A discontinuous galerkin method with lagrange multipliers for the solution of helmholtz problems in the mid-frequency regime, Comput. Methods Appl. Mech. Engrg. 192 (2003) 1389–1419.

[46] C. Farhat, I. Harari, U. Hetmaniuk, The discontinuous enrichment method for multiscale analysis, Comput. Methods Appl. Mech. Engrg. 192 (2003) 3195–3209.

[47] C. Farhat, R. Tezaur, P. Weidemann-Goiran, Higher-order extensions of a discontinuous galerkin method for mid-frequency helmholtz problems, Int. J. Numer. Meth. Engng 61 (2004) 1938–1956.

[48] L. Zhang, R. Tezaur, C. Farhat, The discontinuous enrichment method for elastic wave propagation in the midium-frequency regime, Int. J. Numer. Meth. Engng 66 (2006) 2086–2114.

[49] P. Massimi, R. Tezaur, C. Farhat, A discontinuous enrichment method for three-dimensional multiscale harmonic wave propagation problems in multi-fluid and fluidsolid media, Int. J. Numer. Meth. Engng 76 (2008) 400–425.

[50] C. Farhat, I. Kalashnikova, R. Tezaur, A higher-order discontinuous enrichment method for the solution of high pTclet advectiondiffusion problems on unstructured meshes, Int. J. Numer. Meth. Engng 81 (2010) 604–636.

[51] I. Kalashnikova, R. Tezaur, C. Farhat, A discontinuous enrichment method for variable-coefficient advectiondiffusion at high pTclet number, Int. J. Numer. Meth. Engng 87 (2011) 309–335.

ACCEPTED MANUSCRIPT

ACCEPTED MANUSCRIPT

[52] J. Bedrossian, J. H. von Brecht, S. Zhu, E. Sifakis, J. M. Teran, A second order virtual node method for elliptic problems with interface and irregular domains, J. Comput. Phys. 229 (2010) 6405–6426.

[53] J. Bramble, J. King, A finite element method for interface problems in domains with smooth boundaries and interfaces, Adv. Comput. Math. 6 (1996) 109–138.

[54] Z. Chen, J. Zou, Finite element methods and their convergence for elliptic and parabolic interface problems, Numerische Mathematik 79 (1998) 175–202.

[55] Z. Li, T. Lin, X. Wu, New cartesian grid methods for interface problems using finite element formulation, Numerische Mathematik 96 (2003) 61–98.

[56] C. C. Chu, I. G. Graham, T. Y. Hou, A new multiscale finite element method for high-constrast elliptic interface problems, Mathematics of Computation 79 (2010) 1915–1955.

[57] R. Fedkiw, T. Aslam, B. Merriman, S. Osher, A non-oscillatory eulerian approach to interfaces in multimaterial flows (the ghost fluid method), J. Comput. Phys. 152 (1999) 457–492.

[58] X. Liu, R. Fedkiw, M. Kang, A boundary condition capturing method for poisson's equation on irregular domain, J. Comput. Phys. 160 (2000) 151–178.

[59] F. Gibou, R. P. Fedkiw, L. T. Cheng, M. Kang, A second-order-accurate symmetric discretization of the poisson equation on irregular domains, J. Comput. Phys. 176 (2002) 205–227.

[60] S. Hou, X. Liu, A numerical method for solving variable coefficient elliptic equation with interface, J. Comput. Phys. 202 (2005) 411–445.

[61] R. J. LeVeque, Z. Li, The immersed interface method for elliptic equations with discontinuous coefficients and singular sources, SIAM J. Numer. Anal. 31 (1994) 1019–1044.

[62] S. Deng, K. Ito, Z. Li, Three-dimensional elliptic solvers for interface problems and applications, J. Comput. Phys. 184 (2003) 215–243.

[63] T. Y. Hou, Z. Li, S. Osher, H. Zhao, A hybrid method for moving interface problems with application to the hele-shaw flow, J. Comput. Phys. 134 (1997) 236–252.

[64] L. Adams, Z. Li, The immersed interface/multigrid methods for interface problems, SIAM J. Sci. Comput. 24 (2002) 463–479.

[65] M. A. Dumett, J. P. Keener, An immersed interface method for solving anisotropic elliptic boundary value problems in three dimensions, SIAM J. Sci. Comput. 25 (2003) 348–367.

[66] H. Johansen, P. Colella, A cartesian grid embedded boundary method for poisson's equation on irregular domains, J. Comput. Phys. 147 (1998) 60–85.

ACCEPTED MANUSCRIPT

[67] P. Schwartz, M. Barad, P. Colella, T. Ligocki, A cartesian grid embedded boundary method for the heat equation and poisson's equation in three dimensions, J. Comput. Phys. 211 (2006) 531–550.

[68] M. Oevermann, R. Klein, A cartesian grid finite volume method for elliptic equations with variable coefficients and embedded interafces, J. Comput. Phys. 219 (2006) 749–769.

[69] M. Oevermann, C. Scharfenberg, R. Klein, A sharp interface finite volume method for elliptic equations on cartesian grids, J. Comput. Phys. 228 (2009) 5184–5206.

[70] D. W. Kim, Y. Yoon, W. K. Liu, T. Belytschko, Extrinsic meshfree approximation using asymptotic expansion for interfacial discontinuity of derivative, J. Comput. Phys. 221 (2007) 370–394.

[71] Y. C. Zhou, S. Zhao, M. Feig, G. W. Wei, High order matched interface and boundary method for elliptic equations with discontinuous coefficients and singular sources, J. Comput. Phys. 213 (2006) 1–30.

[72] S. Yu, G. W. Wei, Three-dimensional matched interface and boundary (mib) method for treating geometric singularities, J. Comput. Phys. 227 (2007) 602–632.

[73] T. Belytschko, R. Gracie, G. Ventura, A review of extended/generalized finite element methods for material modeling, Modeling and Simulation in Materials Science and Engineering 17 (2009) 043001.

[74] T. P. Fries, T. Belytschko, The extended/generalized finite element methods: An overview of the method and its applications, Int. J. Numer. Meth. Engng 84 (2010) 253–304.

[75] S. Mohammadi, Extended Finite Element Method for Fracture Analysis of Structures, Blackwell: Oxford, 2008.

[76] C. S. Peskin, The immersed boundary method, Acta Numerica (2002) 479–517.

[77] G. Iaccarino, R. Verzicco, Immersed boundary technique for turbulent flow simulations, Appl. Mech. Rev. 56 (2003) 331–347.

[78] R. Mittal, G. Iaccarino, Immersed boundary methods, Annu. Rev. Fluid Mech. 37 (2005) 239–261.

[79] D. Gottlieb, S. Orszag, Numerical Analysis of Spectral Methods: Theory and Applications, SIAM, Philadelphia, PA, 1977.

[80] J. D. Jackson, Classical Electrodynamics, John Wiley & Sons, Inc, New York, 1998.

[81] R. K. Wangsness, Electromagnetic Fields, John Wiley & Sons, Inc, New York, 1986.

ACCEPTED MANUSCRIPT

[82] J. W. F. Brown, N. H. Frank, E. C. Kemble, W. H. Michener, C. C. Murdock, D. L. Webster, The teaching of electricity and magnetism at the college level: I. logical standards and critical issues, American Journal of Physics 18 (1950) 1–25.

[83] J. W. F. Brown, N. H. Frank, E. C. Kemble, W. H. Michener, C. C. Murdock, D. L. Webster, The teaching of electricity and magnetism at the college level: Ii. two outlines for teachers, American Journal of Physics 18 (1950) 69–88.

[84] A. Ammitzboll, J. M. C. Rauba, M. H. Schultz, N. A. Mortensen, H. Bruus, The dielectrophoretic force on dielectric spherical objects, http://web-files.ait.dtu.dk/bruus/TMF/publications/3week/Jun2006DielectricSphere.pdf (2006).

[85] Y. Nakajima, T. Sato, Calculation of electrostatic force between two charged dielectric spheres by the re-expansion method, Journal of Electrostatics 45 (1999) 213–226.

[86] Y. Chen, A. F. Sprecher, H. Conrad, Electrostatic particle-particle interactions in electrorheological fluids, J. Appl. Phys. 70 (1991) 6796–6803.

[87] P. M. Morse, H. Feshbach, Methods of Theoretical Physics, vol. 2, McGraw-Hill Book Company, Inc., New York, 1953.

[88] P. Moon, D. E. Spencer, Field Theory for Engineers, D. Van Nostrand Company, Inc., Princeton, 1961.

[89] P. R. Nair, P. B. Kumar, R. Sharma, S. Kamohara, S. Mahapatra, A comprehensive trapped charge profiling technique for sonos flash eeproms, IEDM Technical Digest (2005) 403–406.

[90] R. Rodriguez, M. Nafria, J. Sune, X. Aymerich, Analysis of the evolution of the trapped charge distributions in 10nm si02 films during dc and bipolar dynamic stress, Microelectronics Reliability 37 (1997) 1517–1520.

[91] R. W. Sillars, The properties of a dielectric containing semi-conducting particles of various shapes, J Inst Electl Engrs (Lond) 80 (1937) 378–394.

[92] Q. Liu, A stable and accurate projection method on a locally refined staggered mesh, Int. J. Numer. Meth. Fluids 67 (2011) 74–92.

[93] E. Tuncer, Y. V. Serdyuk, S. M. Gubanski, Dielectric mixtures: electrical properties and modeling, IEEE Transactions on Dielectric and Electrical Insulation 9 (2002) 809–828.

ACCEPTED MANUSCRIPT